

# JGR Biogeosciences

## RESEARCH ARTICLE

10.1029/2022JG007077

### Key Points:

- Petrographic and geochemical data constrain molar tooth structure (MTS) development in ~1.57 Ga carbonates from North China
- Microbially induced water column carbonate mud and  $\text{CH}_4$  degassing from the sediment are critical for MTS formation
- The connection between MTS formation and marine oxygenation suggests MTS as a sedimentary redox proxy

### Supporting Information:

Supporting Information may be found in the online version of this article.

### Correspondence to:

D. Tang,  
[dongtang@126.com](mailto:dongtang@126.com)

### Citation:

Tang, D., Fang, H., Shi, X., Liang, L., Zhou, L., Xie, B., et al. (2023). Mesoproterozoic molar tooth structure related to increased marine oxygenation. *Journal of Geophysical Research: Biogeosciences*, 128, e2022JG007077. <https://doi.org/10.1029/2022JG007077>

Received 2 JUL 2022

Accepted 3 JAN 2023

## Mesoproterozoic Molar Tooth Structure Related to Increased Marine Oxygenation

**Dongjie Tang<sup>1,2</sup> , Hao Fang<sup>3</sup>, Xiaoying Shi<sup>1,3</sup>, Liyuan Liang<sup>4</sup> , Limin Zhou<sup>5</sup>, Baozeng Xie<sup>2</sup> , Kangjun Huang<sup>6</sup>, Xiqiang Zhou<sup>7,8</sup>, Mengting Wu<sup>2</sup>, and Robert Riding<sup>4</sup>**

<sup>1</sup>State Key Laboratory of Biogeology and Environmental Geology, China University of Geosciences (Beijing), Beijing, China, <sup>2</sup>Institute of Earth Sciences, China University of Geosciences (Beijing), Beijing, China, <sup>3</sup>School of Earth Sciences and Resources, China University of Geosciences (Beijing), Beijing, China, <sup>4</sup>Department of Earth and Planetary Sciences, University of Tennessee, Knoxville, TN, USA, <sup>5</sup>National Research Center for Geoanalysis, Beijing, China, <sup>6</sup>State Key Laboratory for Continental Dynamics and Early Life Institute, Department of Geology, Northwest University, Xi'an, China, <sup>7</sup>Key Laboratory of Cenozoic Geology and Environment, Institute of Geology and Geophysics, Chinese Academy of Sciences, Beijing, China, <sup>8</sup>College of Earth and Planetary Sciences, University of Chinese Academy of Sciences, Beijing, China

**Abstract** Marine carbonate fabrics are intrinsically related to ocean chemistry, physical processes and biological activity. Molar tooth structure (MTS), a globally distributed structure in Proterozoic carbonate sediments, has been widely studied for more than a century; yet its connections with physical and biological processes remain unclear. Using multiple techniques, we studied ~1.57 Ga MTS and identified a connection between its occurrence and increased marine oxygenation. In our samples, the matrix surrounding MTS is typically dominated by carbonate mud with early diagenetic dolomite crystals. High  $\text{I}/(\text{Ca} + \text{Mg})$  ratios (up to 4.1  $\mu\text{mol/mol}$ ) and negative Ce anomalies (~−0.8) detected in the matrix are consistent with the oxidative removal of inhibitors such as  $\text{Fe}^{2+}$  and  $\text{Mn}^{2+}$  in the water-column that permitted carbonate “whiting” mud precipitation stimulated by cyanobacterial photosynthesis. This cohesive but not rigid seafloor carbonate mud was a prerequisite for synsedimentary MTS crack formation. Systematically higher carbon isotope ( $\delta^{13}\text{C}$ ) values in MTS microspars, relative to host sediment, support origination of the cracks by methane degassing in the organic-rich carbonate mud. Low, but non-zero,  $\text{I}/(\text{Ca} + \text{Mg})$  values of the MTS microspar suggest that the precipitation of the microspar that filled the MTS cracks was triggered by oxidative removal of residual  $\text{Fe}^{2+}$  and  $\text{Mn}^{2+}$  in porewater through mixing with overlying oxygenated seawater. We therefore propose that MTS formed under moderately oxygenated conditions and that its sporadic occurrence prior to ~1.2 Ga reflects episodes of pulsed marine oxygenation in an overall anoxic setting.

**Plain Language Summary** Molar tooth structure (MTS) has been identified in Precambrian carbonate sedimentary rocks for more than a century. However, its formation and significance are still not fully understood. Precambrian ocean chemistry and low oxygen levels have previously been linked to MTS formation. Here, we use carbonate iodine data as a proxy for oxygenation, and carbon isotope data to decipher microbial processes. The iodine data indicate an oxygenated environment, and the carbon isotope data support previous suggestions that degassing of microbial methane was responsible for MTS crack formation. For the first time, we show that MTS occurred in oxygenated conditions. We propose that the oxidative removal of ions such as  $\text{Fe}^{2+}$  and  $\text{Mn}^{2+}$  that can inhibit carbonate precipitation was a key factor in the formation of the cohesive carbonate mud matrix of MTS, and in the rapid precipitation of the microspar cement that filled and preserved the MTS cracks. The relatively rare occurrence of MTS prior to 1,200 Ma could therefore be a sedimentary indicator of sporadic marine oxygenation when marine conditions were mostly anoxic.

### 1. Introduction

Molar tooth structure (MTS), characterized by irregular, lobate folds of microspar-filled cracks in fine-grained carbonate rocks, has been studied for more than a century, yet its origin is still not fully resolved (Hodgskiss et al., 2018; Kuang & Hu, 2014; Shields, 2002). MTS is locally common during the interval 2,500–1,200 million years ago (Ma), abundant in ~1,200–750 Ma, and relatively rare after ~750 Ma (Hodgskiss et al., 2018; Kriscautzky et al., 2022; Pollock et al., 2006; Pratt, 1998; Shields, 2002). Three processes are thought to characterize MTS

formation: (a) precipitation of carbonate mud and its seafloor accumulation, (b) crack formation within this carbonate mud matrix, and (c) synsedimentary crack-filling by microspar (e.g., Hodgskiss et al., 2018; Shen et al., 2016).

Sources for Proterozoic carbonate mud could include water column “whittings” of physicochemical origin (Pratt, 1998) or stimulated by cyanobacterial photosynthesis (Riding, 2006), skeletal disaggregation of calcified green algae (Gischler & Zingeler, 2002; Tosti & Riding, 2017), and grain abrasion (Trower et al., 2019). Secular increase in carbonate mud accumulation during the Proterozoic has been attributed to increase in photo-synthetically induced whiting production in the water column (Grotzinger, 1989, 1990; Knoll & Swett, 1990; Sherman et al., 2000; Sumner & Grotzinger, 2004; Swett & Knoll, 1985), triggered by the oxidative removal of  $\text{Fe}^{2+}$  and  $\text{Mn}^{2+}$  from the water-column, and the effect of declined  $\text{CO}_2$  on cyanobacterial photosynthesis (Konhauser & Riding, 2012; Riding, 2006). It was suggested that the abundance of carbonate precipitation inhibitors (e.g.,  $\text{Fe}^{2+}$  and  $\text{Mn}^{2+}$ ) in ferruginous seawater suppresses crystal nuclei formation and carbonate crystallization, thereby maintaining a supersaturated solution that limits carbonate mud precipitation in the water column (Sumner & Grotzinger, 1996). Moreover, shallow seawater oxygenation may have increased aerobic respiration of organic matter ( $\text{O}_2 + \text{CH}_2\text{O} \rightarrow \text{CO}_2 + \text{H}_2\text{O} \leftrightarrow \text{HCO}_3^- + \text{H}^+$ ), causing a decline in  $\text{CaCO}_3$  saturation near the sediment-water interface, which in turn hindered seafloor precipitation and tended to maintain soft and unconsolidated seafloor sediment (Higgins et al., 2009). Considering these effects, the formation of MTS may potentially be linked to marine oxygenation.

Suggested mechanisms for crack formation, such as subaqueous syneresis (Horodyski, 1983; Knoll, 1984) and seismic activity (Fairchild et al., 1997; Pratt, 1998), do not appear to account for the long-term secular distribution of MTS. Gas bubble expansion including  $\text{H}_2\text{S}$  (Furniss et al., 1998) or  $\text{CO}_2$  (Marshall & Anglin, 2004; Pollock et al., 2006; Saha et al., 2021) degassing, could be involved. However, the generally low sulfate concentrations widely inferred for Proterozoic shallow seawater (Kah et al., 2004; Luo et al., 2015; Spear et al., 2014) may not have produced sufficient  $\text{H}_2\text{S}$  in sediment, and elevated  $\text{CO}_2$  degassing could promote calcite dissolution rather than precipitation. Shen et al. (2016) linked methanogenesis during widespread euxinic conditions to  $\text{CH}_4$  degassing and crack formation. This would require euxinic bottom water and an adequate sulfate reservoir. However, current assessments suggest that Proterozoic shallow seawater was characterized by low sulfate concentrations (Kah et al., 2004; Luo et al., 2015; Spear et al., 2014), with ferruginous conditions predominant below a redoxcline (Planavsky et al., 2011; Poulton & Canfield, 2011). Furthermore, it is likely that at least some MTS formed in oxygenated settings, for example, in the ~1.57 Ga Gaoyuzhuang Formation, North China (Fang et al., 2022; Shang et al., 2019; K. Zhang et al., 2018). Volume reduction in clay mineral transformation induced by microbial dissimilatory iron reduction during early diagenesis could assist crack formation (Hodgskiss et al., 2018). However, abundant clay minerals appear uncommon in most MTS host rocks (Bishop et al., 2006; Saha et al., 2021).

Rapid filling by microspar is widely regarded as a key process in the preservation of MTS cracks. Dissolved organic molecules, produced by organic matter decomposition, could have initiated MTS microspar precipitation as the pore fluids mixed with supersaturated Proterozoic seawater (Pollock et al., 2006). Mixing of seawater with porewater containing slightly elevated  $\text{Ca}^{2+}$  concentrations may have induced carbonate nucleation, thereby promoting subsequent crystal growth (Bishop et al., 2006). Alternatively, other studies suggest that this was likely caused by increased alkalinity or pH in sediments during methanogenesis (Shen et al., 2016), dissimilatory iron reduction (Hodgskiss et al., 2018), or  $\text{CO}_2$  degassing (Saha et al., 2021). None of these mechanisms, however, appears to be sufficiently time-limited to account for the observed mid–late Proterozoic distribution of MTS, or for characteristic features of MTS formation such as the generation of cracks within unconsolidated sediment and their rapid infilling with microspar prior to sediment compaction (Hodgskiss et al., 2018; Kuang & Hu, 2014).

In order to further elucidate the origin of MTS, we used multiple techniques to determine petrographic and geochemical parameters, including  $\text{I}/(\text{Ca} + \text{Mg})$  and carbon isotope values, associated with MTS from the ~1.57 Ga Gaoyuzhuang Formation in the Jixian area of North China (Figure 1). These results shed new light on MTS genesis and its possible relationship with seawater redox variation in the early Mesoproterozoic.

## 2. Geological Setting

Proterozoic sediments are well-preserved at Jixian, ~100 km to the east of Beijing, China (Figure 1), in a sedimentary succession up to ~9 km thick atop Archean–Paleoproterozoic crystalline basement (Tosti & Riding, 2017).

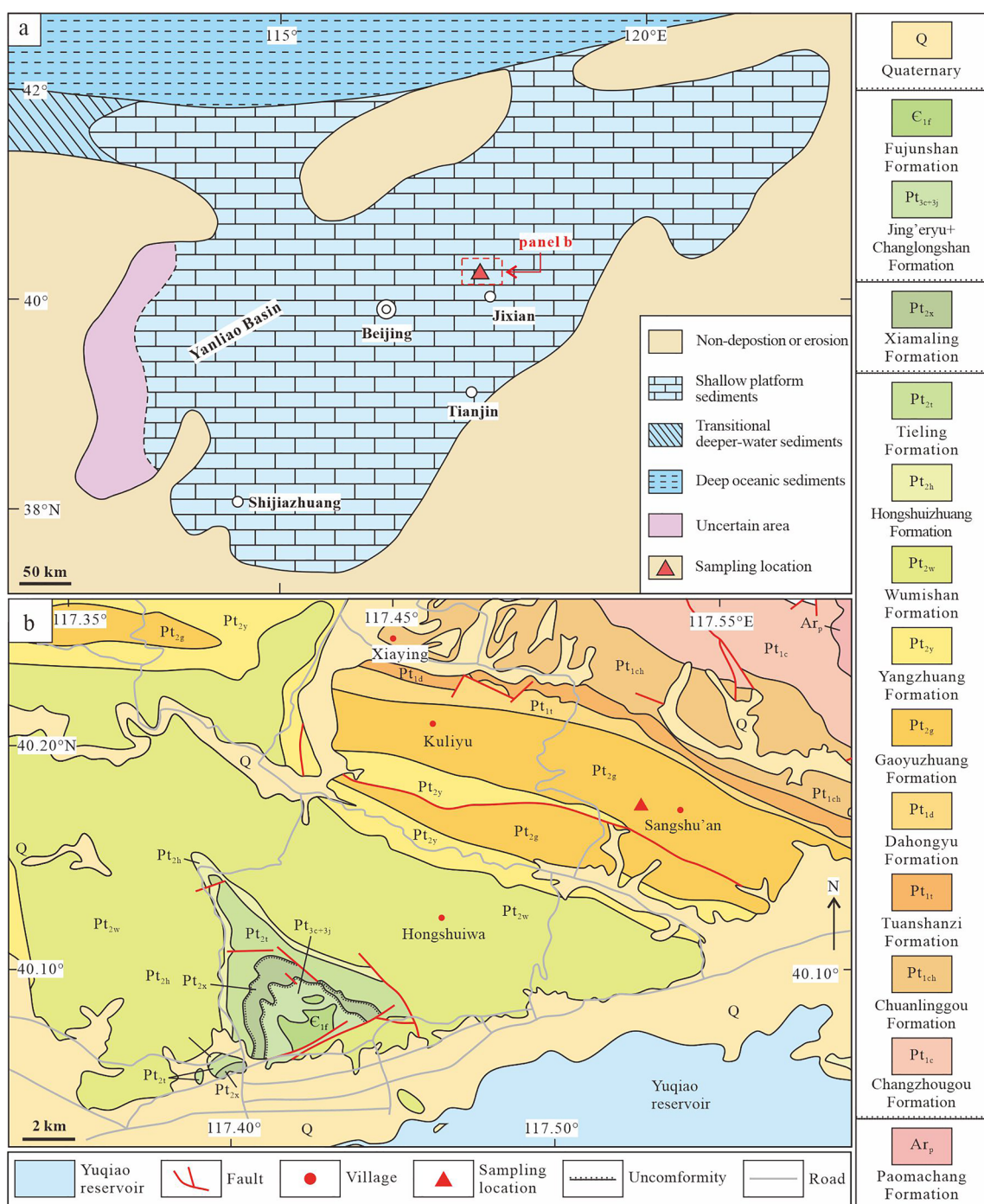


**Figure 1.** Geological setting. (a) Simplified ~1.7 to 1.4 Ga paleogeographic map of the North China Platform (modified after H. Wang et al., 1985). (b) Simplified geological map of the study area, and the locality of the studied section (modified from HBGMR, 1965).

The Early Mesoproterozoic Gaoyuzhuang Formation consists mainly of shallow marine carbonate, ranging from deep shelf to supratidal (K. Zhang et al., 2018), and is traditionally sub-divided into four members (Figure 2). Member I consists mainly of medium to thick-bedded dolostone with stromatolites and chert bands (Fang et al., 2020; K. Zhang et al., 2018). Member II is characterized by thin to medium-bedded Mn-rich muddy dolostone and shale at the base, and medium to thick-bedded dolostone in the upper part, commonly with interference ripple marks (Fang et al., 2020). Member III is dominated by medium to thick-bedded limestone and dolomitic limestone, containing well-preserved MTS, stromatolites, and limestone concretions. Wave- or current-agitated

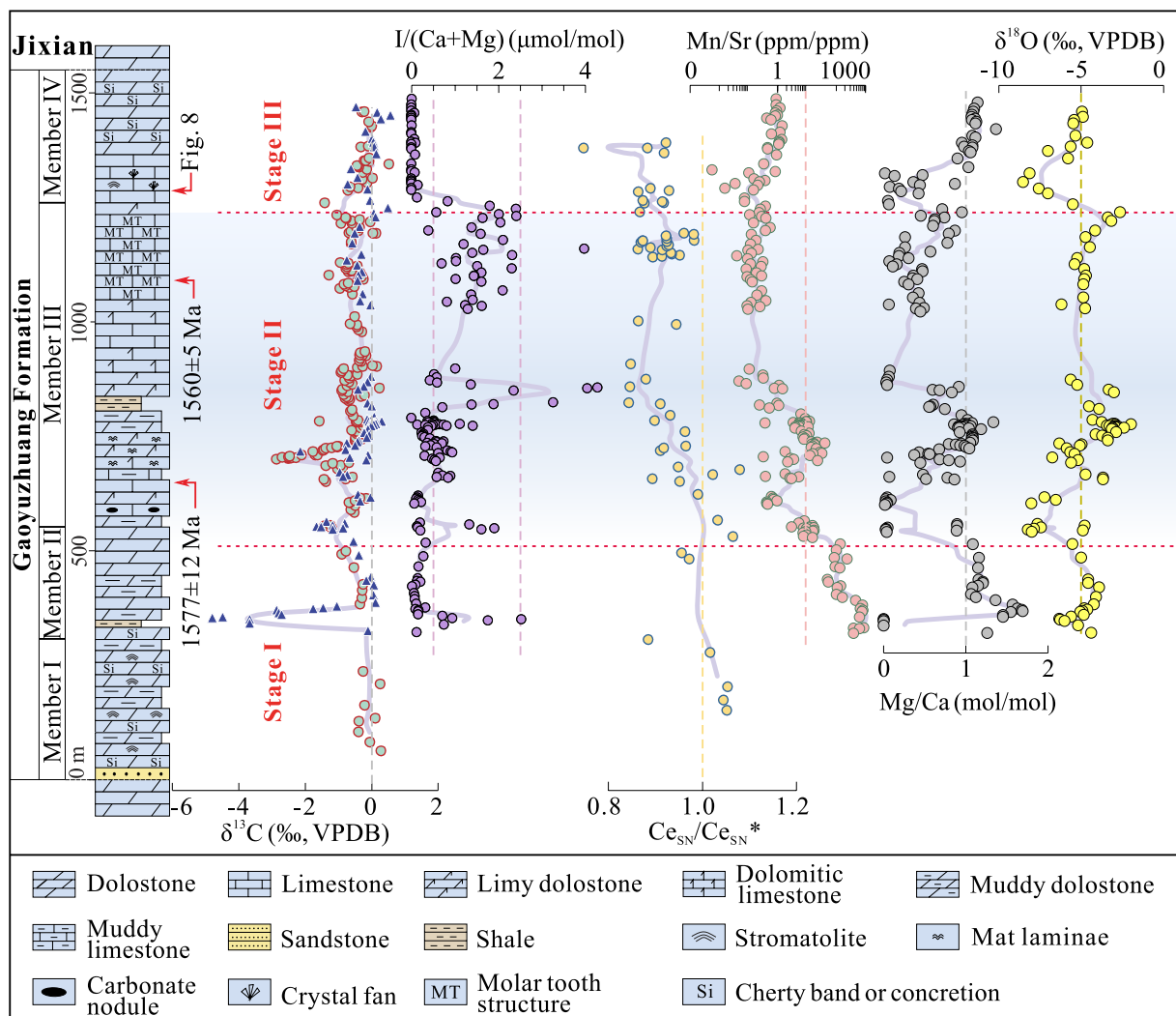


**Figure 2.** Stratigraphic column of the Gaoyuzhuang Formation in the Jixian section with compiled  $\delta^{13}\text{C}$  (circles, K. Zhang et al., 2018; triangles, this study),  $\text{I}/(\text{Ca} + \text{Mg})$  ratios, Ce anomaly profile (K. Zhang et al., 2018), Mn/Sr ratios, Mg/Ca ratios, and  $\delta^{18}\text{O}$  measured in carbonate rocks. The lines through the data represent a 5-point running average.

sedimentary structures are occasionally observed in the upper part (Fang et al., 2020; K. Zhang et al., 2018). Member IV comprises massive microbialites alternating with medium to thick-bedded dolostone (Mei, 2005; Tang et al., 2016). Seafloor crystal fans composed of acicular aragonite are abundant in the lower part of this member (Fang et al., 2022; Wu et al., 2021). U-Pb zircon dating of tuff beds in the lower and upper horizons of Member III (Figure 2) yields ages of  $1,577 \pm 12$  Ma (Tian et al., 2015) and  $1,560 \pm 5$  Ma (H. Li et al., 2010), respectively.

### 3. Samples and Methods

We collected 186 carbonate samples from throughout the Gaoyuzhuang Formation in the Jixian section ( $40^{\circ}09'2.09''\text{N}$  and  $117^{\circ}28'34.32''\text{E}$ ). In addition, MTS samples ( $n = 25$ ) from Member III, and crystal fans ( $n = 44$ ) and carbonate mud samples ( $n = 10$ ) from Member IV were also collected for comparison. Petrography and mineralogy of thin-sections of the samples containing MTS were analyzed using light microscopy and field emission scanning electron microscopy with energy disperse spectroscopy (EDS; Tang et al., 2017). The mineralogy of the crack filling and matrix in MTS was further investigated using X-ray diffraction (XRD), following the methods described in Tang et al. (2017).

Iodine in carbonate samples was determined using MC-ICP-MS, whereas Ca, Mg, Al, Mn, and Sr were analyzed using ICP-MS at the National Research Center for Geoanalysis, Beijing, following the method described in Shang et al. (2019). The detection limit of iodine was on the order of 0.02 ppm. The analytical uncertainty of iodine monitored by the standard GSR-12 and duplicate samples is  $\leq 7\%$ . The analytical uncertainties monitored by JDo-1 were  $<3\%$  for Mg and  $<2\%$  for Ca.

A stepwise dissolution method was conducted using a 50-mg host rock sample as follows. Depending on Ca and Mg content, 0.1% v/v nitric acid was added to the selected sample and its duplicate samples. Following 0.5-hr digestion in an ultrasonic bath, the supernatant was transferred to fresh centrifuge tubes and diluted to  $\sim 1:6,000$ , following the method described in Shang et al. (2019). Digestion and supernatant transfer were repeated 10 times, and an extra step was followed to examine the residual carbonate. Iodine concentration and Mg/Ca ratios from each step (i.e., stepwise dissolution) were analyzed following the method described in Shang et al. (2019).

Carbonate carbon and oxygen isotopes were analyzed on a gas bench and isotope ratio mass spectrometer (Delta-V Advantage) at Northwest University, in Xi'an, following the method described in P. Zhang et al. (2022). Two standard samples were added every six sample-interval for monitoring and correction. Analytical precision was better than  $\pm 0.1\text{‰}$  for  $\delta^{13}\text{C}$  and  $\pm 0.2\text{‰}$  for  $\delta^{18}\text{O}$  (VPDB), as monitored by IAEA CO<sub>2</sub> ( $\delta^{13}\text{C} = -5.8\text{‰}$ ;  $\delta^{18}\text{O} = -22.7\text{‰}$ ), GBW04405 ( $\delta^{13}\text{C} = -0.6\text{‰}$ ;  $\delta^{18}\text{O} = -8.5\text{‰}$ ), and calcite ( $\delta^{13}\text{C} = -13.8\text{‰}$ ;  $\delta^{18}\text{O} = -27.7\text{‰}$ ).

## 4. Results

### 4.1. Secular Variations

Based on carbonate I/(Ca + Mg) values ( $n = 166$ ), the geochemical evolution of the Gaoyuzhuang Formation in the Jixian section can be sub-divided into three successive stages that show significantly pulsed increase (Figure 2, Table S1). In Stage I (Member I to upper Member II), the I/(Ca + Mg) values of most samples (19/24) are lower than 0.5  $\mu\text{mol/mol}$ . This level is suggested as a baseline for Proterozoic carbonate and was confirmed by more than 95% of Proterozoic samples deposited in suboxic–anoxic settings (Hardisty et al., 2017; W. Lu et al., 2017; Shang et al., 2019). The other 5 samples show higher I/(Ca + Mg) ratios, up to 2.4  $\mu\text{mol/mol}$ , and are from a Mn-rich layer in the basal Member II (Fang et al., 2020). In Stage II (uppermost Member II and Member III), most samples (72/111) have I/(Ca + Mg) values above 0.5  $\mu\text{mol/mol}$ , with a maximum up to 4.1  $\mu\text{mol/mol}$ . In Stage III (Member IV), all the samples have I/(Ca + Mg) values below 0.5  $\mu\text{mol/mol}$ .

The short-lived pulse of increased I/(Ca + Mg) in Stage I is associated with a negative  $\delta^{13}\text{C}$  excursion down to  $-5.0\text{‰}$ . However, this excursion was interpreted as the result of early diagenesis (Fang et al., 2020). The significant increase of I/(Ca + Mg) observed in Stage II is accompanied by  $\delta^{13}\text{C}$  values down to  $-2.3\text{‰}$ , which are also recognized in many other sections across the Yanliao basin (Shang et al., 2019; K. Zhang et al., 2018).

Mg/Ca molar ratios are low (average 0.61 mol/mol,  $n = 111$ ) in Stage II, and higher in Stage I (average 1.04 mol/mol,  $n = 24$ ) and Stage III (average 0.80 mol/mol,  $n = 31$ ). No obvious co-variation is observed between I/(Ca + Mg) and Mg/Ca (Figure 3a). Mn/Sr ratios are very high in Stage I, the Mn-rich interval in Member II (average 358.7,  $n = 30$ ), but generally lower in Stage II (average 5.6,  $n = 115$ ) and Stage III (average 0.7,  $n = 31$ ; Figure 2, Table S1). Measured  $\delta^{18}\text{O}$  values from this formation are commonly higher than  $-10\text{‰}$ . Furthermore, I/(Ca + Mg) ratios do not obviously covary either with  $\delta^{18}\text{O}$ , or with Sr and Al (Figures 3b–3d).

### 4.2. Micro-Fabric Features of MTS

In plan view on bedding surfaces, MTS occurs as irregular microspar-filled ribbon-like voids, several mm to tens of cm in size, with pointed terminations (Figures 4a and 4b). In vertical profile, they display ptygmatically folded ribbon-like shapes, vertical or variably oblique to bedding. Two shapes are common: (a) blunt top with sharply pointed base; and (b) sharply pointed top and base (Figure 4c). It is possible that some of the pointed tops are not true terminations, but reflect irregular cracks that continue upward beyond the plane of section. Microspar ribbons often show somewhat rigid fractures (Figure 4d), and are associated with depressions in the associated laminated sediment (Figures 4e and 4f). The cracks are filled with microspar calcite crystals, typically 10–20  $\mu\text{m}$  in size (Figure 4g). The host rock is composed mainly of fine-grained partially dolomitized carbonate mud with moderate silification, as shown by XRD analysis (Figure 5a). The dolomite grains often have a low-Fe center and relatively high-Fe boundary as indicated by EDS (Figure 5b, Table S2). Consistent with the geochemical data

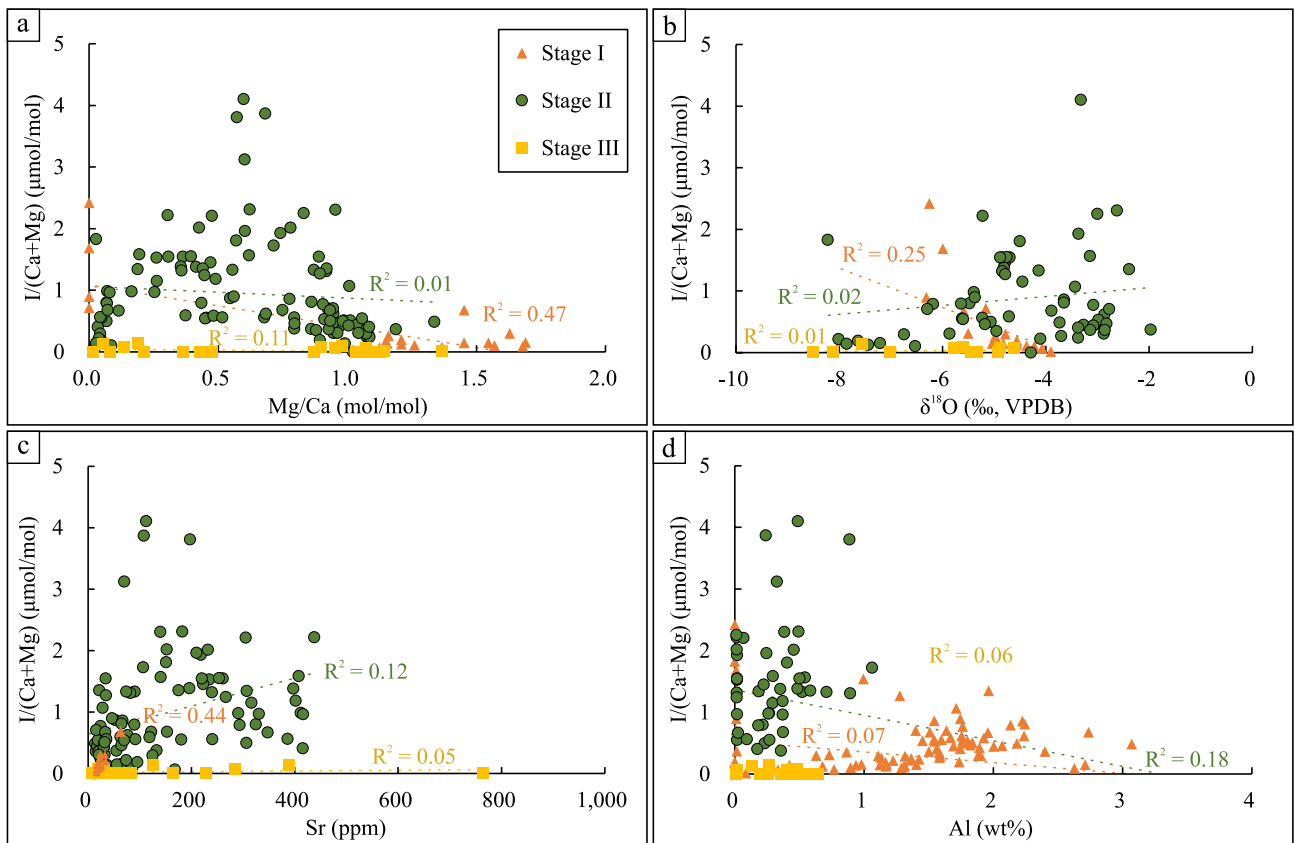


**Figure 3.** Measured I/(Ca + Mg) values for samples from the Gaoyuzhuang Formation are plotted for Stages I–III (see main text for discussion). The I/(Ca + Mg) values do not show obvious correlations with (a) Mg/Ca, (b) δ<sup>18</sup>O, (c) Mn/Sr, or (d) Al for Stages II and III. Only the Stage I I/(Ca + Mg) data show moderate correlation with Sr, followed by Mg/Ca and δ<sup>18</sup>O.

(Figure 5), backscatter electron and cathodoluminescence images show that the calcite crystals in both crack and host rock are non-luminescent, indicative of negligible Fe or Mn incorporation, whereas the dolomite in the host rock has dull-luminescence, indicating some Fe or Mn incorporation (Figure 6).

Average I/(Ca + Mg) values in the host rock of MTS are significantly higher than 0.5 μmol/mol ( $0.95 \pm 0.46$ ,  $n = 25$ ), whereas those in the microspar are typically less than 0.5 μmol/mol but higher than 0 μmol/mol ( $0.10 \pm 0.17$ ,  $n = 25$ ; Figure 5c, Table S3). Stepwise dissolution of the host rock shows high I/(Ca + Mg) values (average 4.27 μmol/mol,  $n = 3$ ) at low Mg/Ca ratios (calcite, average 0.30 mol/mol,  $n = 3$ ), and relatively low I/(Ca + Mg) values (dolomite, average 1.60 μmol/mol,  $n = 3$ ) at high Mg/Ca ratios (average 0.94 mol/mol,  $n = 3$ ) (Figures 5d and 5e, Table S4). Average δ<sup>13</sup>C values of the crack filling microspars ( $+0.4 \pm 0.4\text{‰}$ ,  $n = 25$ ) are systematically heavier than those in the neighboring host rock ( $-0.2 \pm 0.2\text{‰}$ ,  $n = 25$ ; Figure 5f, Table S3). δ<sup>18</sup>O and δ<sup>13</sup>C values are not correlated in cross-plots (Figure 7a). I/(Ca + Mg) ratios in the carbonate do not covary with Mg/Ca, δ<sup>18</sup>O, Mn/Sr, or Al, but are positively correlated with iodine content (Figures 7b–7f).

#### 4.3. Water-Column Whitings and Seafloor Precipitation

Seafloor precipitated aragonite crystal fans and interbedded carbonate muds co-occur in the lower part of Member IV (Figure 2; Fang et al., 2022). These contrasting fabrics provide a window into the origin of the carbonate mud. The crystal fan-bearing interval can be up to 10 m in thickness. Crystal fans commonly appear as compressed discs and are occasionally interrupted by centimeter to decimeter thick carbonate mud layers (Figures 3a and 3b in Fang et al., 2022) that show variable thickness laterally (Figure 3a in Fang et al., 2022). The crystal fans are up to 20 cm in diameter and have long axes up to 10 cm in length (Figures 3c, 3d and 4 in Fang et al., 2022). They are all now calcite but consist of radiating fibers with square terminations typical of aragonite (Figures 3c, 3d, 4 and 5a in Fang et al., 2022) rather than gypsum or calcite. Individual crystals in the fans commonly are ~1 mm in width, and increase slightly in width from bottom to top (Figures 5a and 5b in Fang et al., 2022). Layers adjacent

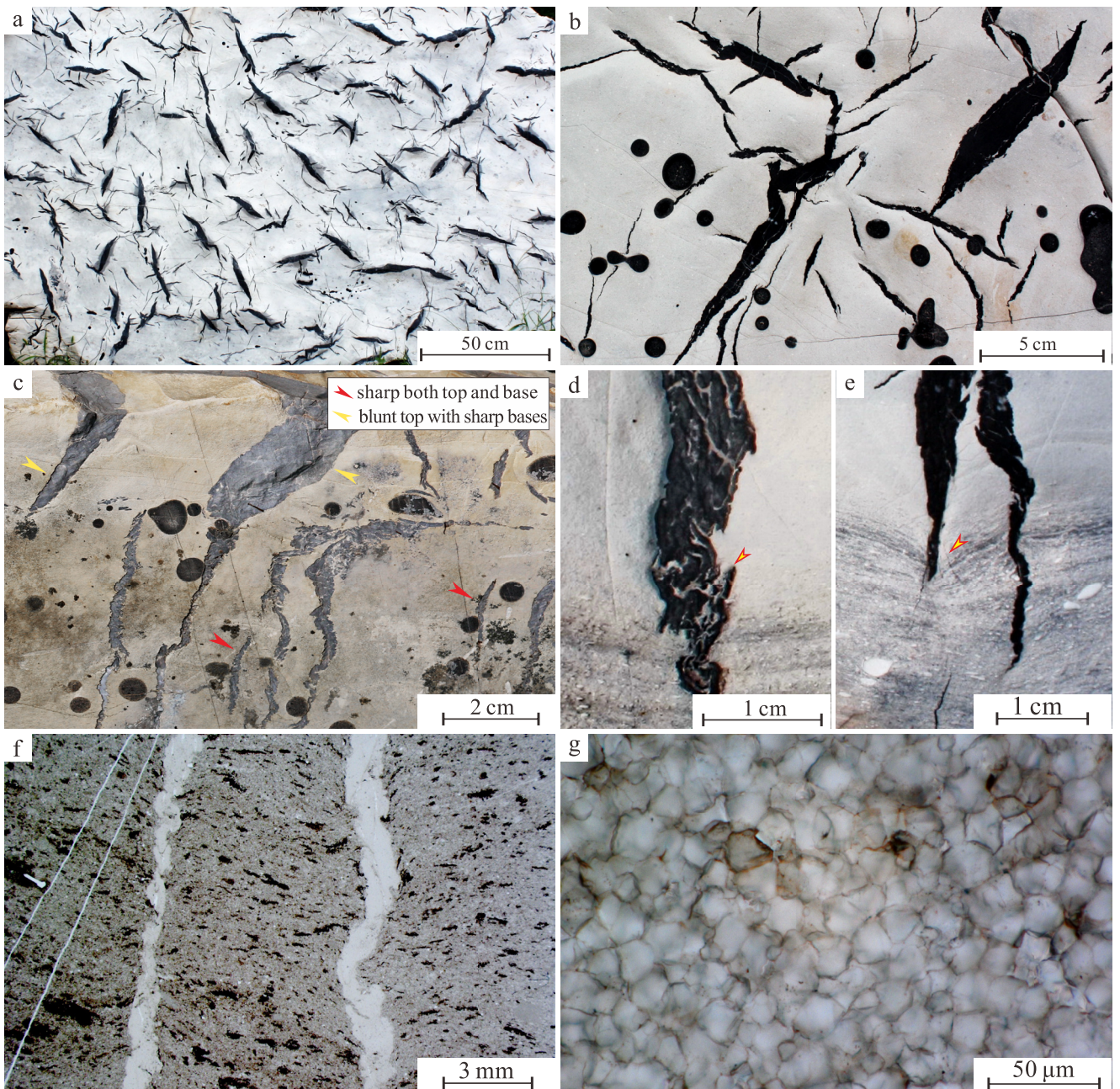


**Figure 4.** Macroscopic and microscopic features of the Gaoyuzhuang molar tooth structure (MTS). (a and b) Plan views of MTS, the small black circles are chert nodules; (c–e) vertical views of MTS, showing two morphologic types: MTS with both sharp top and base (red arrows) and MTS with blunt top and sharp base (yellow arrows). (d) Arrow indicates partially rigid fractures. (e) Arrow indicates downward bending lamination near the crack base. (f) Detail showing microspar filled ptygmatic cracks. (g) High magnification image showing 10–20  $\mu\text{m}$  microspar grains.

to the crystal fans typically are composed of ~20  $\mu\text{m}$  sized calcite grains (Figure 5c in Fang et al., 2022), which are interpreted to have precipitated from water column as small “whiting” crystals (see discussion in Section 5.3).

The crystal fans have relatively high Sr concentration, ranging from 51 to 2,021 ppm (average 679,  $n = 42$ ; Table S5), consistent with primary aragonite mineralogy.  $\delta^{13}\text{C}$  values of the crystal fans average  $-0.4\text{\textperthousand} \pm 0.2\text{\textperthousand}$  ( $n = 44$ ; Figure 8a, Table S5), and generally lower than the adjacent carbonate mud layers (average  $+0.2\text{\textperthousand} \pm 0.6\text{\textperthousand}$ ;  $n = 10$ ; Figure 8a, Table S5). Average  $\delta^{18}\text{O}$  values of the crystal fans and carbonate mud layers are  $-8.0\text{\textperthousand} \pm 0.6\text{\textperthousand}$  ( $n = 44$ ; Table S5) and  $-7.8\text{\textperthousand} \pm 0.5\text{\textperthousand}$  ( $n = 10$ ; Table S5), respectively, and show no obvious correlation with  $\delta^{13}\text{C}$  (Figure 8b).

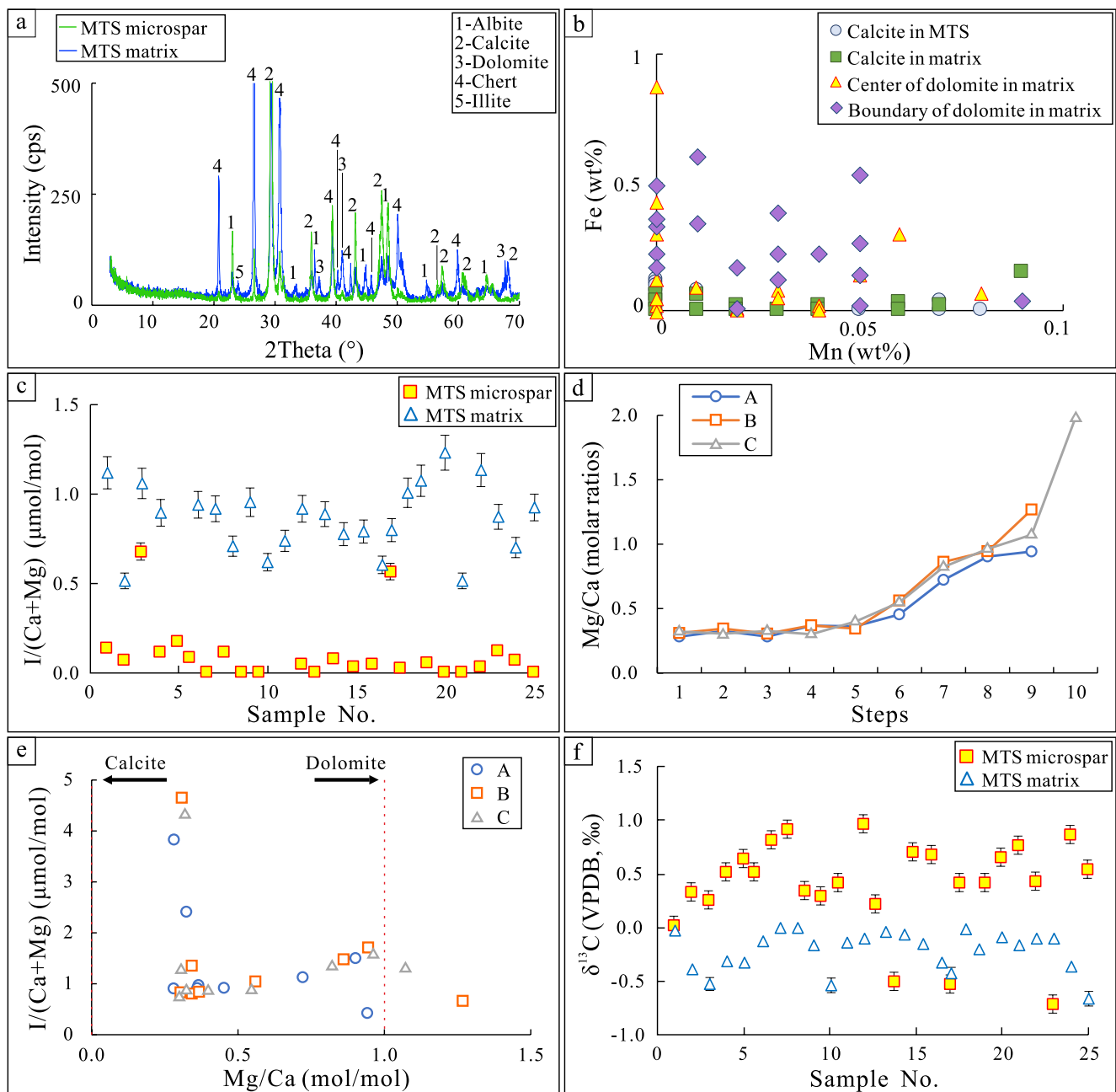


**Figure 5.** Mineralogy and geochemical compositions of the Gaoyuzhuang molar tooth structure (MTS). (a) X-ray diffraction analysis results for microspar and host matrix in MTS, showing that MTS microspar is “pure” calcite, whereas the MTS matrix experienced dolomitization and silicification. (b) Quantitative energy disperse spectroscopy analysis results for microspar and host rock (the relative uncertainty is  $<\pm 3\%$ ). (c)  $I/(Ca + Mg)$  of microspar and host rock (error  $<\pm 8\%$ ). (d) Results of stepwise dissolution of MTS host rock, showing that Mg/Ca molar ratios increase with dissolution. Three parallel experiments are shown as A, B, and C. (e) Correlation of  $I/(Ca + Mg)$  and Mg/Ca, showing high  $I/(Ca + Mg)$  values in calcite and relatively low  $I/(Ca + Mg)$  in dolomite. Replicate experiments are shown as A, B, and C. (f)  $\delta^{13}\text{C}$  of microspar and host rock (error  $<\pm 0.1\%$ ).

## 5. Discussion

### 5.1. Variation in Redox Conditions

$I/(Ca + Mg)$  ratio in carbonate is considered a significant proxy for seawater redox conditions and has been widely applied in studies of ancient carbonate rocks younger than  $\sim 2.5$  Ga (Hardisty et al., 2014, 2017; Z. Lu et al., 2010; W. Lu et al., 2018; Shang et al., 2019). Since metamorphism and diagenetic alteration can affect

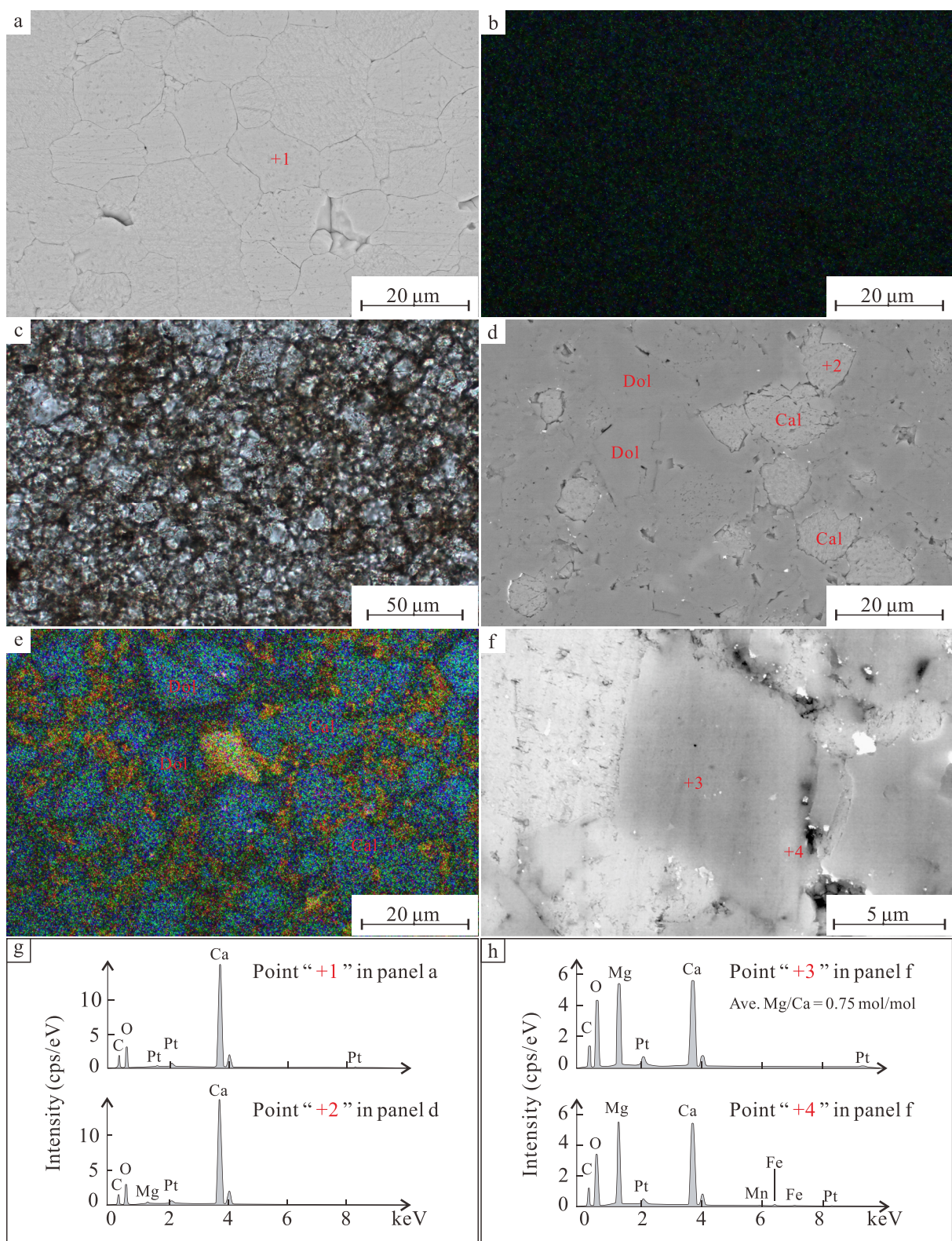


**Figure 6.** Microscopic features of Gaoyuzhuang molar tooth structure (MTS). (a) High magnification backscatter electron (BSE) image, showing calcite microspar 10–20 µm in size. (b) Cathodoluminescence (CL) image of the same area as panel a, showing non-luminescence of calcite. (c) Carbonate mud in MTS-host rock. (d) BSE image showing areas of calcite (Cal) muds in dolomite (Dol) matrix. (e) CL image of the same area as panel (d), showing non-luminescence of calcite and dull-luminescence dolomite. (f) BSE image showing a dolomite grain with a dark nucleus and relatively light rim. (g) Energy disperse spectroscopy (EDS) analysis result of calcite in panels (a and d). (h) EDS analysis result of the center and margin of the dolomite in panel (f), showing some Fe and Mn in the margin.

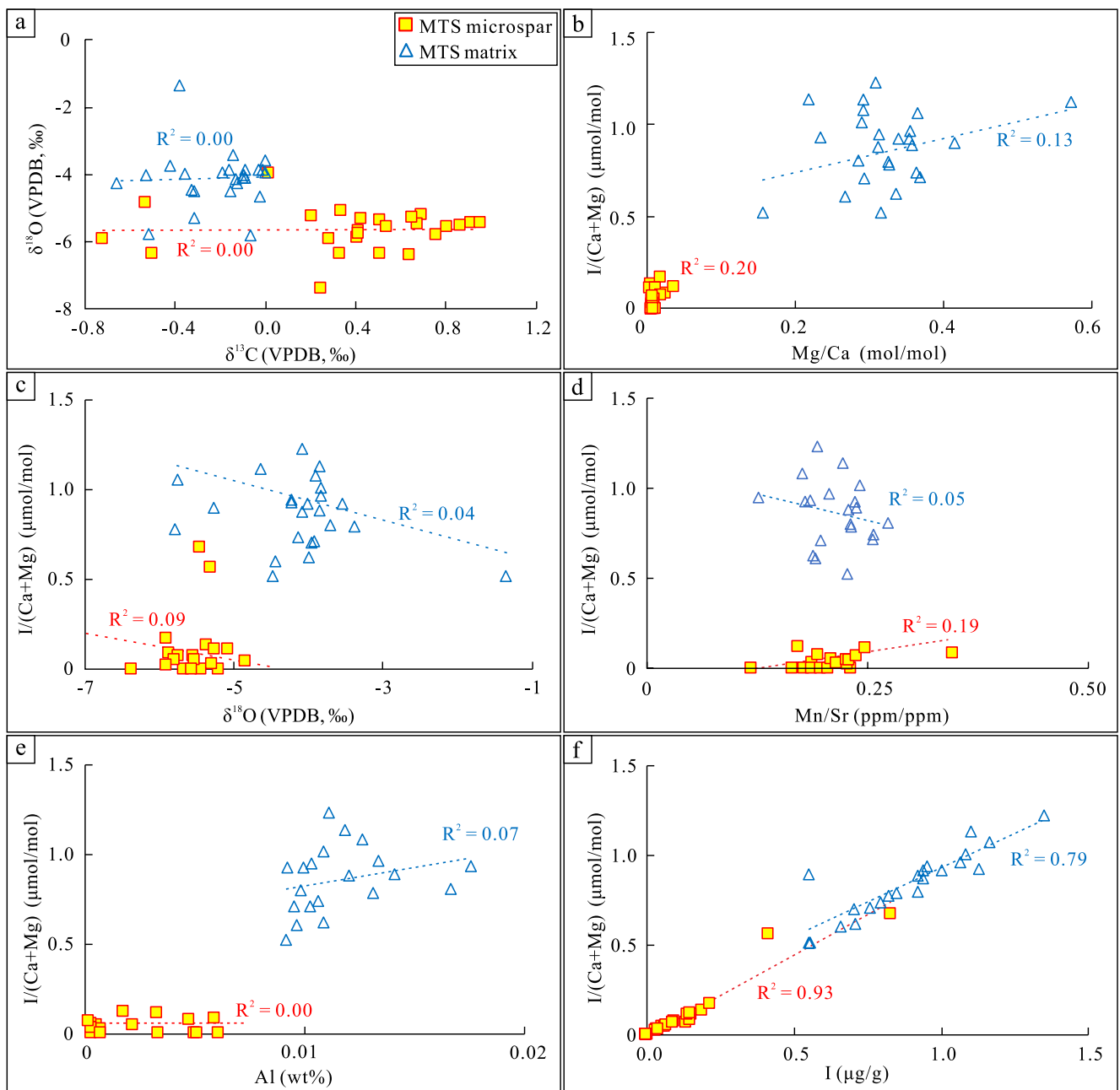


**Figure 7.** Geochemical analysis data for Gaoyuzhuang molar tooth structure (MTS). (a)  $\delta^{13}\text{C}$  versus  $\delta^{18}\text{O}$  of MTS microspar and host rock.  $I/(Ca + Mg)$  as a function of (b)  $Mg/Ca$ , (c)  $\delta^{18}\text{O}$ , (d)  $Mn/Sr$ , (e)  $Al$ , and (f)  $I$ . No obvious correlations exist in panel (a) through panel (e), except for panel (f) where positive correlation between  $I/(Ca + Mg)$  and  $I$  is observed.

$I/(Ca + Mg)$  ratios in carbonate rocks (e.g., Hardisty et al., 2014, 2017; Z. Lu et al., 2010; W. Lu et al., 2018; Shang et al., 2019), the degree of alteration should be evaluated before applying  $I/(Ca + Mg)$  to redox condition analysis. In the Jixian section, the metamorphic grade of the Gaoyuzhuang Formation is low, generally below prehnite-pumpellyite facies (Chu et al., 2007; C. Li et al., 2003). Calcite crystals in the host rocks of MTS generally are small ( $\sim 10 \mu\text{m}$ ), lack obvious secondary overgrowth, and show non- to dull-luminescence (Figure 6), suggesting insignificant recrystallization. Meteoric diagenesis could significantly lower  $\delta^{18}\text{O}$  values (Halverson et al., 2007) and commonly decreases Sr, but can increase Mn content in carbonate rocks (Brand & Veizer, 1980). In our case, most of the samples have  $>-10\text{‰}$   $\delta^{18}\text{O}$  values and low Mn/Sr ratios ( $<\sim 2\text{--}3$ ), indicative of weak meteoric alteration (Kaufman & Knoll, 1995). Although the Mn-rich interval in the lower Member II has a high

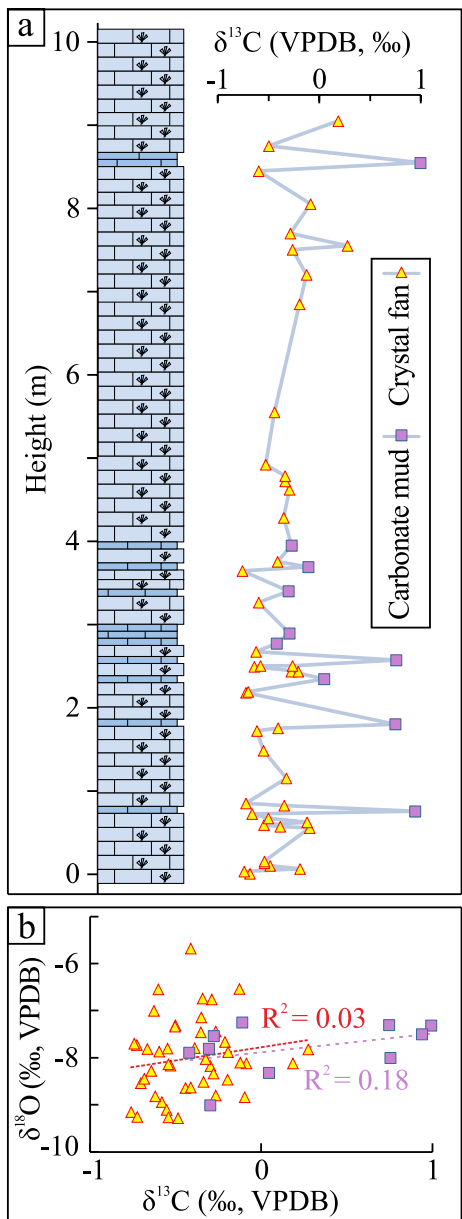


**Figure 8.** (a)  $\delta^{13}\text{C}$  values of seafloor aragonite crystal fans and calcite carbonate muds from a 10 m thick interval from the base of Member IV of the Gaoyuzhuang Formation. (b) Plot of aragonite and calcite  $\delta^{18}\text{O}$  versus  $\delta^{13}\text{C}$  values in panel (a).

If the Mesoproterozoic ocean experienced similar iodine cycling to that of the modern ocean, then the observed increase of  $\text{I}/(\text{Ca} + \text{Mg})$  to 4.1  $\mu\text{mol/mol}$  in Stage II (Figure 2) may possibly indicate oxygen concentrations  $>20\text{--}70 \mu\text{M}$  (cf. Z. Lu et al., 2016).

## 5.2. Redox Conditions of Seafloor and Porewater

In addition to carbonate mud precipitated from the water-column, euhedral dolomite crystals that precipitated from porewater are also present in the MTS matrix, providing an opportunity to assess seafloor redox conditions. Dolomite crystals in MTS matrix appear to have been formed during early diagenesis, since they occur as matrix supporting whiting calcite mud. Microscopic observations reveal rim-core structure in the dolomite euhedral

Mn/Sr ratio, this has been attributed to pulsed increase in oxygen, rather than to diagenesis (Fang et al., 2020). Furthermore, the  $\text{I}/(\text{Ca} + \text{Mg})$  ratios do not show obvious correlation with  $\text{Mg/Ca}$ ,  $\delta^{18}\text{O}$ , and Sr or Al (Figure 3), suggesting that  $\text{I}/(\text{Ca} + \text{Mg})$  ratios in the carbonate mainly reflect iodine content in seawater rather than either dolomitization, diagenetic processes, or the presence of terrestrial clay (cf. Hardisty et al., 2017; Wörndle et al., 2019).

Iodine can exist as iodide ( $\text{I}^-$ ) and iodate ( $\text{IO}_3^-$ ) in seawater, and only iodate is incorporated into the carbonate lattice, whereas iodide is excluded (Feng & Redfern, 2018; Z. Lu et al., 2010, 2016). Studies of modern ocean oxygen minimum zones indicate that oxidized iodate species are stable only in oxic surface water, and will be reduced to iodide in oxygen-depleted conditions (Emerson et al., 1979; Luther & Campbell, 1991). Furthermore, since diagenetic fluids commonly have low iodate concentrations, early diagenesis and late-stage alteration would decrease rather than increase the iodate concentration in carbonate (Hardisty et al., 2017; Z. Lu et al., 2010; Wörndle et al., 2019). It follows that high  $\text{I}/(\text{Ca} + \text{Mg})$  ratio generally indicates a high oxygen concentration in seawater (Z. Lu et al., 2010). Our  $\text{I}/(\text{Ca} + \text{Mg})$  data show a marked increase from  $<0.5 \mu\text{mol/mol}$  in Stage I to 4.1  $\mu\text{mol/mol}$  in middle Stage II, followed by an abrupt fall in Stage III, suggestive of pulsed oxygenation during Stage II (Figure 2). This is supported by associated negative Ce anomalies in Stage II ( $\text{Ce}/\text{Ce}^* = \sim 0.8$ ; K. Zhang et al., 2018), implying that Gaoyuzhuang MTS mainly formed during enhanced oxygenation. Recognition of oxygenation in stage II and deoxygenation in stage III is also supported by the mineralogical transformation reflected in the contrast between water-column precipitated calcitic mud and seafloor precipitated aragonite crystal fan, modulated by the absence or presence of  $\text{Fe}(\text{II})$  and  $\text{Mn}(\text{II})$  that can influence carbonate precipitation in seawater (Fang et al., 2022).

Compilation of available carbonate  $\text{I}/(\text{Ca} + \text{Mg})$  data and comparison of iodine cycling in modern oceans show that this proxy can be used to further constrain seawater oxygen concentrations semi-quantitatively (Hardisty et al., 2017; Shang et al., 2019). Non-zero  $\text{I}/(\text{Ca} + \text{Mg})$  values could indicate the presence of iodate in seawater and oxygen concentrations higher than 1–3  $\mu\text{M}$  (Hardisty et al., 2014, 2017). In our case, most samples (50/55) from Stage I and Stage III have  $\text{I}/(\text{Ca} + \text{Mg})$  values lower than the Proterozoic baseline (0.5  $\mu\text{mol/mol}$ ; W. Lu et al., 2017; Shang et al., 2019) but higher than zero, suggesting that during Stages I and III carbonate rocks were deposited under weakly oxygenated (suboxic-anoxic) conditions, with oxygen concentrations higher than 1–3  $\mu\text{M}$  but less than 10  $\mu\text{M}$  (cf. A. Liu et al., 2020; Reinhard et al., 2016; Wei et al., 2021). According to studies of modern anoxic basins (Hardisty et al., 2017; Z. Lu et al., 2016),  $\text{I}/(\text{Ca} + \text{Mg}) > 2.6 \mu\text{mol/mol}$  may be used as an indicator of water column oxygen concentration  $>20\text{--}70 \mu\text{M}$  (Hardisty et al., 2017; Shang et al., 2019).

crystals, with relatively enriched Fe and Mn in the rims (Figures 6f and 6h). This could suggest that the dolomite crystals were secondarily enlarged by porewater in a Mn-Fe reduction zone during early diagenesis. If so, the dolomite matrix has the potential to reflect the redox conditions in the seafloor porewater.

Stepwise dissolution of the MTS matrix shows that, during this process, the dolomite endmember is commonly dissolved later than the calcite (Figure 5d). I/(Ca + Mg) in the dolomite (Mg/Ca molar ratio = 1) is  $\sim 1.6 \mu\text{mol}/\text{mol}$ ; significantly lower than that of the calcite ( $\sim 4.3 \mu\text{mol}/\text{mol}$ ) but higher than zero (Figure 5e). We therefore infer that the dolomite formed in suboxic shallow porewater, whereas the carbonate mud likely precipitated in the water-column under oxic conditions. It should be noted that dolomitization commonly causes decrease in I/(Ca + Mg) (Wörndle et al., 2019), therefore the dolomite likely formed in more oxygenated conditions than the present-day conserved estimation.

Partially rigid fractures in the MTS cracks, and the downward bending laminae beneath them, indicate that the voids formed after deposition of the matrix, but prior to subsequent filling by microspar precipitation (Figures 4d and 4e). The low I/(Ca + Mg) values ( $\sim 0.1 \mu\text{mol}/\text{mol}$ ) of the calcite microspar in the MTS voids are unlikely to have been produced by intense diagenetic alteration, since the calcite carbonate mud in the matrix has very high I/(Ca + Mg) (Figure 5e). Thus, the low I/(Ca + Mg) values of the MTS microspar suggest that the crack fills precipitated under suboxic ambient conditions. We therefore infer that the MTS formed during early diagenesis and that the void-filling microspar likely formed when deep porewater mixed with oxic-suboxic bottom seawater. Since this was a rapid process, iodide would not have been oxidized to iodate and incorporated into the microspar (cf. Luther et al., 1995), resulting in low I/(Ca + Mg) ratios in MTS microspar.

### 5.3. Origin of Carbonate Mud Matrix

The presence of soft unconsolidated carbonate mud was a prerequisite for MTS formation, since it provided the matrix that was subsequently prone to synsedimentary cracking (Riding, 2006). In our samples, unaltered calcite mud is preserved as areas  $\sim 5\text{--}20 \mu\text{m}$  in size surrounded by dolomite matrix (Figure 6d). A plausible origin for abundant Mesoproterozoic carbonate mud is precipitation stimulated by cyanobacterial photosynthesis (Riding, 2006). Origins of present-day abundant carbonate mud include (a) disintegration of tropical calcified green algae such as *Penicillus* (Lowenstam & Epstein, 1957), (b) water column “whittings” driven by cyanobacterial photosynthetic bicarbonate uptake (Thompson & Ferris, 1990), and/or (c) inorganic precipitation (Milliman et al., 1993). It can be hypothesized that, in the Precambrian, heterogeneous nucleation of carbonate mud in the water column might occur without photosynthetic stimulation during time intervals and/or in locations of elevated marine saturation for CaCO<sub>3</sub> minerals (Grotzinger, 1989; Knoll & Swett, 1990). These conditions could also be expected to favor the precipitation of seafloor crusts. Current evidence and estimates suggest that multicellular green algae did not emerge until  $\sim 1$  Ga (Tang et al., 2020). Based on this information, and assuming that green algae may not have been present  $\sim 1,500$  Ma, we suggest that the origin of the abundant fine-grained carbonate sediment observed in our samples was likely due to heterogeneous nucleation of carbonate in the water-column, promoted by elevated saturation levels and/or a photosynthetic stimulus, as suggested previously (Riding, 2006; Tosti & Riding, 2017).

Previous studies have suggested that Precambrian abundance of water-column precipitated carbonate mud increased with shallow seawater oxygenation (Sumner & Grotzinger, 1996). This trend of secular increase could be ascribed to the increase in oxygenation of seawater and decrease in atmospheric CO<sub>2</sub> levels (e.g., Fang et al., 2022; Riding, 2006; Tosti & Riding, 2017; Wu et al., 2021). Laboratory experiments suggest that under anoxic conditions, carbonate precipitation inhibitors (such as 0.02  $\mu\text{M}$  Fe<sup>2+</sup> and 3  $\mu\text{M}$  Mn<sup>2+</sup>) can lower the rates of crystal nuclei formation and crystallization, leading to kinetic maintenance of supersaturated solutions (Meyer, 1984). It was also suggested that this effect could hinder micritic carbonate precipitation in the water column but permit aragonite growth of seafloor crystal fans (Sumner & Grotzinger, 1996). It therefore follows that oxidative removal of Fe<sup>2+</sup> and Mn<sup>2+</sup> from the water column could promote the formation of carbonate mud under conditions of elevated carbonate-saturation. Coeval decrease in atmospheric CO<sub>2</sub> levels could also have played a significant role. Cyanobacterial calcification could suggest Late Mesoproterozoic CO<sub>2</sub> concentrations  $<\sim 12 \times$  preindustrial atmospheric levels (Kah & Riding, 2007; Riding, 2006). Under these conditions, cyanobacteria are likely to utilize bicarbonate (HCO<sub>3</sub><sup>-</sup>) as an additional carbon source (Riding, 2006). During this process, transformation of absorbed HCO<sub>3</sub><sup>-</sup> to CO<sub>2</sub> would release OH<sup>-</sup>, leading to localized relatively high pH conditions that could promote nucleation and growth of CaCO<sub>3</sub> on and around the cyanobacterial cell (Kah &

Riding, 2007; Riding, 2006). As a result, blooms of picoplanktic cyanobacteria in shallow water could result in rapid precipitation of fine-grained carbonate (“whitings”) in the water column leading to copious accumulation of fine-grained carbonate sediment (Riding, 2006; Tosti & Riding, 2017).

Differences in inorganic carbon isotope values between the crystal fans and interbedded carbonate mud layers provide further evidence for cyanobacterial involvement in the carbonate mud precipitation. Our data show an average  $\delta^{13}\text{C}$  of  $+0.2\text{\textperthousand} \pm 0.6\text{\textperthousand}$  ( $n = 10$ ) in the carbonate mud and  $-0.4\text{\textperthousand} \pm 0.2\text{\textperthousand}$  ( $n = 44$ ) in the crystal fans throughout a  $\sim 10$  m thick interval at the base of Member IV of the Gaoyuzhuang Formation (Figure 8). Assuming that the aragonite crystal fans precipitated abiotically on the seafloor, as in the Archean (Sumner & Grotzinger, 1996), variations in seawater carbon isotopes can be inferred. Using the constant fractionation of  $\sim +2.7\text{\textperthousand} \pm 0.6\text{\textperthousand}$  between aragonite crystal fan and bicarbonate in seawater (Romanek et al., 1992), the  $\delta^{13}\text{C}$  of bicarbonate in seawater ( $\text{DIC}_{\text{seawater}}$ ) in this study would be  $\sim -3.1\text{\textperthousand}$ . Since the transformation of aragonite to calcite commonly occurs in a closed diagenetic system at relatively elevated temperature and pressure, the effect of transformation on the carbon isotope value would be negligible (cf. Swart, 2008). In contrast, based on the fractionation constant ( $+1.0\text{\textperthousand} \pm 0.2\text{\textperthousand}$ ) between calcite and bicarbonate (Romanek et al., 1992), the  $\delta^{13}\text{C}$  of DIC for the formation of carbonate mud should be  $\sim -0.8\text{\textperthousand}$ , which is higher than that of  $\text{DIC}_{\text{seawater}}$  ( $\sim -3.1\text{\textperthousand}$ ) by  $\sim +2.3\text{\textperthousand}$ . This could be caused by the surface-to-deep ocean  $\delta^{13}\text{C}$  gradient (cf. Jiang et al., 2007), and/or by cyanobacterial mediation (cf. Pentecost & Spiro, 1990; Thompson et al., 1997). The stable composition of carbonate carbon isotopes during the early Mesoproterozoic suggests a relatively large marine DIC with small surface-to-deep water  $\delta^{13}\text{C}$  gradient (cf. Bartley & Kah, 2004). Therefore, the observed changes in our samples could possibly reflect the preferential uptake of light carbon in photosynthesis, thereby leaving heavier carbon in the micro-environment surrounding the picoplanktic cyanobacteria (Pentecost & Spiro, 1990; Thompson et al., 1997).

Oxygenation of bottom water could be conducive to the maintenance of unconsolidated sediment during early diagenesis (cf. Higgins et al., 2009), whereas anoxic degradation of settling organic matter by anaerobes could increase pH in porewater, promoting early cementation. Thus, suboxic to oxic conditions could favor soft substrate and retard early lithification, facilitating crack formation in MTS. We therefore infer that in the presence of dissolved  $\text{O}_2$ , aerobic degradation of settling organic matter ( $\text{O}_2 + \text{CH}_2\text{O} \rightarrow \text{CO}_2 + \text{H}_2\text{O} \leftrightarrow \text{HCO}_3^- + \text{H}^+$ ) may have produced net acidity, thereby decreasing pH in seafloor porewaters and slowing sediment cementation (Figure 9). The low organic content in the MTS-hosting carbonate would favor the maintenance of suboxic porewater conditions. In contrast, a high concentration of organic matter would rapidly exhaust oxygen in porewater and result in transition from aerobic respiration to anaerobic respiration, and thus early cementation. The conclusion that this scenario would not facilitate MTS crack formation is supported by studies of the relatively organic-rich Gaoyuzhuang Formation, where MTS is absent (e.g., Yanqing section) (Shang et al., 2019; Tang et al., 2022).

#### 5.4. Origin of MTS Crack and Microspar Filling

Ocean chemistry-related gas bubbling provides a feasible mechanism for MTS crack formation. It is unlikely that the cracks resulted from  $\text{H}_2\text{S}$  degassing, since  $\text{SO}_4^{2-}$  concentrations appear to have been too low in Mesoproterozoic seawater to allow bacterial sulfate reduction to generate sufficient  $\text{H}_2\text{S}$  (Fakhraee et al., 2019; Kah et al., 2004; Luo et al., 2015). The scarcity of authigenic pyrite in the Gaoyuzhuang Formation could further support this interpretation (Shang et al., 2019; Z. Wang et al., 2020). In addition, Gaoyuzhuang MTS formed in an oxygenated setting (Figure 2; Shang et al., 2019; K. Zhang et al., 2018).  $\text{CO}_2$ -degassing also seems unlikely, since bacterial fermentation tends to decrease pH, hindering calcite formation. The MTS cracks are more likely to have been produced by microbial  $\text{CH}_4$  generation and degassing (cf. Shen et al., 2016; Figure 9b). In modern oceans,  $\text{CH}_4$  generated during early diagenesis would largely be consumed through anaerobic oxidation of methane via reaction:  $\text{CH}_4 + \text{SO}_4^{2-} \rightarrow \text{HS}^- + \text{HCO}_3^- + \text{H}_2\text{O}$ , thereby limiting  $\text{CH}_4$  accumulation in sediment (Knittel & Boetius, 2009). In contrast, in the Early Mesoproterozoic ocean, the reconstructed seawater sulfate concentrations were very low (<2 mM), based on multiple sulfur isotope compositions analyzed for paired carbonate-associated sulfate and disseminated pyrite (Luo et al., 2015). Modeling based on mass balance and diagenetic reaction-transport calculations also suggests <0.4 mM sulfate concentration (Fakhraee et al., 2019). These low sulfate concentrations, compared with 28 mM in the modern oceans, make methane accumulation in the sediment feasible.

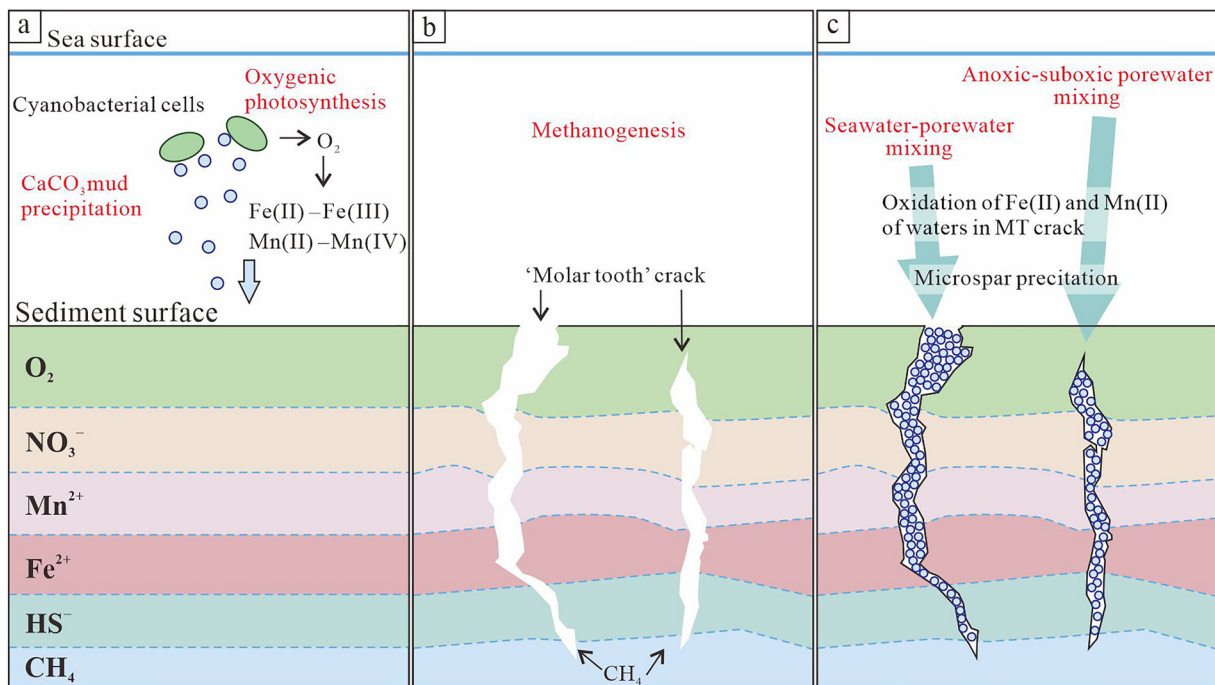


**Figure 9.** Three-step model of Gaoyuzhuang molar tooth structure (MTS) formation: carbonate mud precipitation, MTS crack formation, crack-filling by microspar. (a) Photosynthetic uptake of bicarbonate by picoplanktic cyanobacteria promoted water column “whiting” nucleation of  $CaCO_3$ . Simultaneously, oxygenation removed dissolved  $Fe^{2+}$  and  $Mn^{2+}$  inhibitors of calcite precipitation. As a result, “whiting” mud, rich in organic matter, accumulated. (b) Methane, produced by methanogens processing the organic-rich carbonate mud, created MTS cracks in soft but sufficiently cohesive sediment. The sinuous crack morphology could reflect early compaction following precipitation of MTS microspar. (c) Mixing of alkaline,  $Fe^{2+}$  and  $Mn^{2+}$  rich pore fluids with moderately oxygenated seawater and porewater, resulted in removal of  $Fe^{2+}$  and  $Mn^{2+}$  from water within the MTS crack, triggering calcite microspar precipitation that filled the crack, thereby preserving the MTS.

Methanogenesis was suggested as a key mechanism for the generation of MTS (Furniss et al., 1998; Shen et al., 2016). This model invokes microspar enriched in  $\delta^{13}C$  by  $0.5\text{‰}$ – $1.0\text{‰}$  relative to the host rock as evidence for methanogenesis. However, in many cases there appears to be no clear difference in carbon isotope composition between MTS microspar and the host sediment (Hodgskiss et al., 2018). This discrepancy might be resolved if the  $\delta^{13}C$  value of the carbonate mud in MTS-hosting carbonate rocks were higher than the equilibrium value between calcite and seawater (by  $\sim+2.3\text{‰}$ ) due to cyanobacterial photosynthesis in the water column (cf. Pentecost & Spiro, 1990; Thompson et al., 1997). In our samples, MTS crack-filling microspar has an average  $\delta^{13}C$  value of  $+0.4\text{‰} \pm 0.4\text{‰}$ , implying that the porewater ( $DIC_{porewater}$ ) from which the microspar precipitated had a  $\delta^{13}C$  value of  $\sim-0.6\text{‰}$ , calculated with a constant fractionation of  $\sim1.0\text{‰}$  between calcite and bicarbonate in water (Romanek et al., 1992). The carbon isotope of the MTS host rock (carbonate mud) is  $-0.2\text{‰} \pm 0.2\text{‰}$ , and that of ambient seawater where the carbonate mud precipitated should therefore have been  $\sim-1.2\text{‰}$ . Since photosynthesis can increase the  $\delta^{13}C$  value of DIC surrounding picoplanktic cyanobacteria by  $\sim+2.3\text{‰}$  (e.g., Pentecost & Spiro, 1990; Thompson et al., 1997), we further infer that the  $\delta^{13}C$  value of the seawater could have been  $\sim-3.5\text{‰}$  in the MTS-bearing interval. The positive shift in  $\delta^{13}C$  values from  $-3.5\text{‰}$  in seawater to  $-0.6\text{‰}$  in porewater could be consistent with methanogenesis occurring in the porewater (cf. Shen et al., 2016). It has been suggested that  $\delta^{13}C$  in the bicarbonate ( $HCO_3^-$ ) generated by methanogenesis is  $\sim-60\text{‰}$  (Summons et al., 1998). If the  $CH_4$ -derived bicarbonate was fully utilized in the formation of microspar, it would only account for  $\sim5\%$  of the microspar formation observed in this study. The relatively low contribution of methanogenesis-derived bicarbonate to microspar precipitation may therefore imply that bottom seawater DIC was significantly (95%) involved in the formation of the microspar.

Early and rapid crack-filling by microspar was critical for MTS preservation. It is possible that the crack-fillings precipitated neither from the water column nor from the host sediment porewater, but formed simultaneously with crack formation through mixing of deep porewater with moderately oxygenated bottom water or shallow porewater (Figure 9c). In these circumstances, cracking itself could be the trigger for rapid microspar precipitation, and this is consistent with relatively high  $I/(Ca + Mg)$  values (Figures 2 and 5e). We therefore propose

the following series of events and conditions during MTS formation in our samples (Figure 9). (a) Planktic cyanobacteria promoted the precipitation of carbonate mud that settled from the water column, seawater oxygenation resulted in the removal of  $\text{Fe}^{2+}$  and  $\text{Mn}^{2+}$  from the water column, and the accumulation of Fe(III)- and Mn(IV)-hydroxides on the seafloor (Figure 9a). (b) Anaerobic reduction during early burial generated  $\text{CH}_4$  gas that created irregular cracks, together with porewater rich in  $\text{Fe}^{2+}$  and  $\text{Mn}^{2+}$  that slowed cementation, although porewater alkalinity and pH could also have been increased by dissimilatory iron and manganese reduction and methanogenesis (Hodgskiss et al., 2018; A. Liu et al., 2019; Shen et al., 2016). This inference is supported by the relatively high Fe(II) and Mn(II) contents of the diagenetic dolomite (Figure 6b). We found no evidence for significant sulfate-fueled anaerobic oxidation of methane in the sediment. Due to the low sulfate concentrations (Fakhraee et al., 2019; Luo et al., 2015), pyrite grains were rare, and the positive  $\delta^{13}\text{C}$  values of MTS microspar are consistent with methanogenesis followed by  $\text{CH}_4$  degassing (Figure 9b). (c) Porewater rich in  $\text{Fe}^{2+}$  and  $\text{Mn}^{2+}$  initially inhibited synsedimentary cementation. However, rapid microspar precipitation within MTS was permitted as cracking exposed these inhibitors to oxidative removal through contact with oxygenated shallow porewater or bottom seawater (Figure 9c), as indicated by low Fe and Mn concentration in MTS microspar (Figure 5b).

## 6. Overview and Implications

Well-developed MTS in the Early Mesoproterozoic Gaoyuzhuang Formation is associated with an oxygenation event supported by high  $\text{I}/(\text{Ca} + \text{Mg})$  ratios and negative Ce anomalies. Oxygenated seawater could have promoted carbonate mud precipitation due to the decrease of carbonate inhibitor ions ( $\text{Fe}^{2+}$  and  $\text{Mn}^{2+}$ ) in the seawater column. This process also slowed seafloor cementation due to the low pH produced by aerobic oxidation of settling organic matter. Systematically higher carbon isotope values in the MTS microspar crystals relative to the host rock indicate that  $\text{CH}_4$  degassing could have created the MTS cracks. The presence of  $\text{Fe}^{2+}$  in the ferruginous porewaters maintained high  $\text{CaCO}_3$  saturation until its removal by mixing with moderately oxygenated seawater. This process likely triggered rapid microspar precipitation within the MTS cracks. The relative scarcity of MTS prior to  $\sim 1.2$  Ga (Kriscautzky et al., 2022; Kuang & Hu, 2014) could therefore correspond with low atmospheric oxygen levels and widespread ocean anoxia (e.g., Cole et al., 2016; X. M. Liu et al., 2021; W. Lu et al., 2018; Lyons et al., 2021; Planavsky et al., 2014; C. Wang et al., 2022). In this view, the occurrence of well-developed MTS in the Gaoyuzhuang Formation may have reflected an episode of increased oxygenation in an otherwise generally anoxic ocean. This explanation could be consistent with identification of Neoarchean MTS (Monteville Formation, Transvaal Supergroup, South Africa; Bishop et al., 2006) in oxygenated setting (cf. Czaja et al., 2012; Wille et al., 2007).

This connection between marine oxygenation and MTS formation suggests MTS as a sedimentary redox proxy. However, in addition to moderately oxygenated seawater, other factors that influence methane gas production, crack formation, and microspar filling are also required for the formation of MTS. For example, too much organic matter would result in a rapid deoxygenation in porewater, and anaerobic degradation of organic matter would lead to increase in pH and alkalinity and, therefore, early seafloor cementation that would inhibit crack formation. The activity of currents in shallow seawater may be important for triggering the MTS crack formation where the cracks were gas-filled and overlain by carbonate mud. An increase in calcite carbonate saturation in shallow seawater through stronger evaporation than that in relatively deep seawater would probably favor rapid filling of MTS cracks. Consequently, the occurrence of MTS was often limited even during intervals of seawater oxygenation. The gradual decline and disappearance of MTS after  $\sim 750$  Ma may reflect secular decrease in carbonate saturation (Pollock et al., 2006), or increase of bioturbation in Phanerozoic (Frank & Lyons, 1998). Further research is required to elucidate these possibilities and uncertainties.

## Data Availability Statement

All geochemical data for this research are available in Supporting Information S1 and at <https://data.mendeley.com/datasets/dh67z28gy7/1>.

## Acknowledgments

This study was supported by a National Key Research and Development Project of China (2020YFA0714803), the National Natural Science Foundation of China (Nos. 41930320 and 41972028), the Key Research Program of the Institute of Geology and Geophysics, CAS (No. IGGCAS-201905), the Chinese “111” project (B20011), and the Fundamental Research Funds for the Central Universities (No. 292019093). The authors appreciate the assistance of Mohan Shang, Yang Li, Haoming Wei, and Zhipeng Wang during fieldwork. The authors are grateful to T. Lyons and M. Pope for perceptive and constructive comments that helped to improve the final text.

## References

- Bartley, J. K., & Kah, L. C. (2004). Marine carbon reservoir,  $C_{org}$ - $C_{carb}$  coupling, and the evolution of the Proterozoic carbon cycle. *Geology*, 32(2), 129–132. <https://doi.org/10.1130/G19939.1>
- Bishop, J. W., Sumner, D. Y., & Huerta, N. J. (2006). Molar tooth structures of the Neoproterozoic Monteville Formation, Transvaal Supergroup, South Africa. II: A wave-induced fluid flow model. *Sedimentology*, 53(5), 1069–1082. <https://doi.org/10.1111/j.1365-3091.2006.00802.x>
- Brand, U., & Veizer, J. (1980). Chemical diagenesis of a multicomponent carbonate system; I, Trace elements. *Journal of Sedimentary Research*, 50(4), 1219–1236. <https://doi.org/10.1306/212FBB7-2B24-11D7-8648000102C1865D>
- Chu, X., Zhang, T., Zhang, Q., & Lyons, T. W. (2007). Sulfur and carbon isotope records from 1700 to 800 Ma carbonates of the Jixian section, northern China: Implications for secular isotope variations in Proterozoic seawater and relationships to global supercontinental events. *Geochimica et Cosmochimica Acta*, 71(19), 4668–4692. <https://doi.org/10.1016/j.gca.2007.07.017>
- Cole, D. B., Reinhard, C. T., Wang, X., Gueguen, B., Halverson, G. P., Gibson, T., et al. (2016). A shale-hosted Cr isotope record of low atmospheric oxygen during the Proterozoic. *Geology*, 44(7), 555–558. <https://doi.org/10.1130/G37787.1>
- Czaja, A. D., Johnson, C. M., Roden, E. E., Beard, B. L., Voegelin, A. R., Nägler, T. F., et al. (2012). Evidence for free oxygen in the Neoproterozoic ocean based on coupled iron-molybdenum isotope fractionation. *Geochimica et Cosmochimica Acta*, 86, 118–137. <https://doi.org/10.1016/j.gca.2012.03.007>
- Emerson, S., Cranston, R. E., & Liss, P. S. (1979). Redox species in a reducing fjord: Equilibrium and kinetic considerations. *Deep Sea Research Part A. Oceanographic Research Papers*, 26(8), 859–878. [https://doi.org/10.1016/0198-0149\(79\)90101-8](https://doi.org/10.1016/0198-0149(79)90101-8)
- Fairchild, I. J., Einsel, G., & Song, T. (1997). Possible seismic origin of molar tooth structures in Neoproterozoic carbonate ramp deposits, north China. *Sedimentology*, 44(4), 611–636. <https://doi.org/10.1046/j.1365-3091.1997.d01-40.x>
- Fakhraee, M., Hancisse, O., Canfield, D. E., Crowe, S. A., & Katsev, S. (2019). Proterozoic seawater sulfate scarcity and the evolution of ocean-atmosphere chemistry. *Nature Geoscience*, 12(5), 375–380. <https://doi.org/10.1038/s41561-019-0351-5>
- Fang, H., Tang, D., Shi, X., Lechte, M., Shang, M., Zhou, X., & Yu, W. (2020). Manganese-rich deposits in the Mesoproterozoic Gaoyuzhuang Formation (ca. 1.58 Ga), North China Platform: Genesis and paleoenvironmental implications. *Paleogeography, Paleoclimatology, Palaeoecology*, 559, 109966. <https://doi.org/10.1016/j.palaeo.2020.109966>
- Fang, H., Tang, D., Shi, X., Zhou, L., Zhou, X., Wu, M., et al. (2022). Early Mesoproterozoic Ca-carbonate precipitates record fluctuations in shallow marine oxygenation. *Precambrian Research*, 373, 106630. <https://doi.org/10.1016/j.precamres.2022.106630>
- Feng, X., & Redfern, S. A. (2018). Iodate in calcite, aragonite and vaterite  $CaCO_3$ : Insights from first-principles calculations and implications for the  $I/Ca$  geochemical proxy. *Geochimica et Cosmochimica Acta*, 236, 351–360. <https://doi.org/10.1016/j.gca.2018.02.017>
- Frank, T. D., & Lyons, T. W. (1998). “Molar-tooth” structures: A geochemical perspective on a Proterozoic enigma. *Geology*, 26(8), 683–686. [https://doi.org/10.1130/0091-7613\(1998\)026<0683:MTSAGP>2.3.CO;2](https://doi.org/10.1130/0091-7613(1998)026<0683:MTSAGP>2.3.CO;2)
- Furniss, G., Ritte, J. F., & Winston, D. (1998). Gas bubble and expansion crack origin of “molar-tooth” calcite structures in the middle Proterozoic Belt Supergroup, western Montana. *Journal of Sedimentary Research*, 68(1), 104–114. <https://doi.org/10.2110/jsr.68.104>
- Gischler, E., & Zingeler, D. (2002). The origin of carbonate mud in isolated carbonate platforms of Belize, Central America. *International Journal of Earth Sciences*, 91(6), 1054–1070. <https://doi.org/10.1007/s00531-002-0288-5>
- Grotzinger, J. P. (1989). Facies and evolution of Precambrian carbonate depositional systems: Emergence of the modern platform archetype. In P. D. Crevello, J. L. Wilson, J. F. Sarg, & J. F. Read (Eds.), *Controls on carbonate platform and basin development* (Vol. 44, pp. 79–106). Special Publication of SEPM (Society of Economic Paleontologists and Mineralogists).
- Grotzinger, J. P. (1990). Geochemical model for Proterozoic stromatolite decline. *American Journal of Science*, 290(80), e103.
- Halverson, G. P., Maloof, A. C., Schrag, D. P., Dudás, F. Ö., & Hurtgen, M. (2007). Stratigraphy and geochemistry of a ca 800 Ma negative carbon isotope interval in northeastern Svalbard. *Chemical Geology*, 237(1–2), 5–27. <https://doi.org/10.1016/j.chemgeo.2006.06.013>
- Hardisty, D. S., Lu, Z., Bekker, A., Diamond, C. W., Gill, B. C., Jiang, G., et al. (2017). Perspectives on Proterozoic surface ocean redox from iodine contents in ancient and recent carbonate. *Earth and Planetary Science Letters*, 463, 159–170. <https://doi.org/10.1016/j.epsl.2017.01.032>
- Hardisty, D. S., Lu, Z., Planavsky, N. J., Bekker, A., Philippot, P., Zhou, X., & Lyons, T. W. (2014). An iodine record of Paleoproterozoic surface ocean oxygenation. *Geology*, 42(7), 619–622. <https://doi.org/10.1130/G35439.1>
- HBGMR (Hebei Bureau of Geology and Mineral Resources). (1965). *Geological map of Xinglong* (K-50-XXXIV, sheet 1, scale 1:200,000). Geological Survey of China. (in Chinese).
- Higgins, J. A., Fischer, W. W., & Schrag, D. P. (2009). Oxygenation of the ocean and sediments: Consequences for the seafloor carbonate factory. *Earth and Planetary Science Letters*, 284(1–2), 25–33. <https://doi.org/10.1016/j.epsl.2009.03.039>
- Hodgkiss, M. S., Kunzmann, M., Poirier, A., & Halverson, G. P. (2018). The role of microbial iron reduction in the formation of Proterozoic molar tooth structures. *Earth and Planetary Science Letters*, 482, 1–11. <https://doi.org/10.1016/j.epsl.2017.10.037>
- Horodyski, R. J. (1983). Sedimentary geology and stromatolites of the middle Proterozoic Belt Supergroup, Glacier National Park, Montana. *Precambrian Research*, 20(2–4), 391–425. [https://doi.org/10.1016/0301-9268\(83\)90083-9](https://doi.org/10.1016/0301-9268(83)90083-9)
- Jiang, G., Kaufman, A. J., Christie-Blick, N., Zhang, S., & Wu, H. (2007). Carbon isotope variability across the Ediacaran Yangtze platform in South China: Implications for a large surface-to-deep ocean  $\delta^{13}C$  gradient. *Earth and Planetary Science Letters*, 261(1–2), 303–320. <https://doi.org/10.1016/j.epsl.2007.07.009>
- Kah, L. C., Lyons, T. W., & Frank, T. D. (2004). Low marine sulphate and protracted oxygenation of the Proterozoic biosphere. *Nature*, 431(7010), 834–838. <https://doi.org/10.1038/nature02974>
- Kah, L. C., & Riding, R. (2007). Mesoproterozoic carbon dioxide levels inferred from calcified cyanobacteria. *Geology*, 35(9), 799–802. <https://doi.org/10.1130/G23680A.1>
- Kaufman, A. J., & Knoll, A. H. (1995). Neoproterozoic variations in the C-isotopic composition of seawater: Stratigraphic and biogeochemical implications. *Precambrian Research*, 73(1–4), 27–49. [https://doi.org/10.1016/0301-9268\(94\)00070-8](https://doi.org/10.1016/0301-9268(94)00070-8)
- Knittel, K., & Boetius, A. (2009). Anaerobic oxidation of methane: Progress with an unknown process. *Annual Review of Microbiology*, 63(1), 311–334. <https://doi.org/10.1146/annurev.micro.61.080706.093130>
- Knoll, A. H. (1984). Microbiotas of the late Precambrian Hunnberg Formation, Nordaustlandet, Svalbard. *Journal of Paleontology*, 58(1), 131–162.
- Knoll, A. H., & Swett, K. (1990). Carbonate deposition during the late Proterozoic Era: An example from Spitsbergen. *American Journal of Science*, 290, 104–132.
- Konhauser, K., & Riding, R. (2012). Bacterial biomineralization. *Fundamentals of Geobiology*, 105–130. <https://doi.org/10.1002/978111820874.ch8>
- Krischautzky, A., Kah, L. C., & Bartley, J. K. (2022). Molar-Tooth Structure as a window into the deposition and diagenesis of Precambrian carbonate. *Annual Review of Earth and Planetary Sciences*, 50(1), 205–230. <https://doi.org/10.1146/annurev-earth-031621-080804>
- Kuang, H. W., & Hu, X. F. (2014). Review of molar tooth structure research. *Journal of Palaeogeography*, 3(4), 359–383. <https://doi.org/10.3724/SP.J.1261.2014.00062>

- Li, C., Sheng, G., Fu, J., & Yan, Y. (2003). A molecular and isotopic geochemical study of Meso-to Neoproterozoic (1.73–0.85 Ga) sediments from the Jixian section, Yanshan Basin, North China. *Precambrian Research*, 125(3–4), 337–356. [https://doi.org/10.1016/S0301-9268\(03\)00111-6](https://doi.org/10.1016/S0301-9268(03)00111-6)
- Li, H., Zhu, S., Xiang, Z., Su, W., Lu, S., Zhou, H., et al. (2010). Zircon U-Pb dating on tuff bed from Gaoyuzhuang Formation in Yanqing, Beijing: Further constraints on the new subdivision of the Mesoproterozoic stratigraphy in the northern North China Craton. *Acta Petrologica Sinica*, 26(7), 2131–2140. (in Chinese with English abstract).
- Liu, A., Tang, D., Shi, X., Zhou, L., Zhou, X., Shang, M., et al. (2019). Growth mechanisms and environmental implications of carbonate concretions from the ~1.4 Ga Xiamaling Formation, North China. *Journal of Palaeogeography*, 8(1), 1–16. <https://doi.org/10.1186/s42501-019-0036-4>
- Liu, A., Tang, D., Shi, X., Zhou, X., Zhou, L., Shang, M., et al. (2020). Mesoproterozoic oxygenated deep seawater recorded by early diagenetic carbonate concretions from the Member IV of the Xiamaling Formation, North China. *Precambrian Research*, 341, 105667. <https://doi.org/10.1016/j.precamres.2020.105667>
- Liu, X. M., Kah, L. C., Knoll, A. H., Cui, H., Wang, C., Bekker, A., & Hazen, R. M. (2021). A persistently low level of atmospheric oxygen in Earth's middle age. *Nature Communications*, 12(1), 1–7. <https://doi.org/10.1038/s41467-020-20484-7>
- Lowenstam, H. A., & Epstein, S. (1957). On the origin of sedimentary aragonite needles of the Great Bahama Bank. *The Journal of Geology*, 65(4), 364–375. <https://doi.org/10.1086/626439>
- Lu, W., Ridgwell, A., Thomas, E., Hardisty, D. S., Luo, G., Algeo, T. J., et al. (2018). Late inception of a resiliently oxygenated upper ocean. *Science*, 361(6398), 174–177. <https://doi.org/10.1126/science.aar5372>
- Lu, W., Wörndl, S., Halverson, G. P., Zhou, X., Bekker, A., Rainbird, R. H., et al. (2017). Iodine proxy evidence for increased ocean oxygenation during the Bitter Springs Anomaly. *Geochemical Perspectives Letters*, 5, 53–57. <https://doi.org/10.7185/geochemlet.1746>
- Lu, Z., Hoogakker, B. A., Hillenbrand, C. D., Zhou, X., Thomas, E., Gutches, K. M., et al. (2016). Oxygen depletion recorded in upper waters of the glacial Southern Ocean. *Nature Communications*, 7(1), 1–9. <https://doi.org/10.1038/ncomms11146>
- Lu, Z., Jenkyns, H. C., & Rickaby, R. E. (2010). Iodine to calcium ratios in marine carbonate as a paleo-redox proxy during oceanic anoxic events. *Geology*, 38(12), 1107–1110. <https://doi.org/10.1130/G31145.1>
- Luo, G., Ono, S., Huang, J., Algeo, T. J., Li, C., Zhou, L., et al. (2015). Decline in oceanic sulfate levels during the early Mesoproterozoic. *Precambrian Research*, 258, 36–47. <https://doi.org/10.1016/j.precamres.2014.12.014>
- Luther, G. W., III, & Campbell, T. (1991). Iodine speciation in the water column of the Black Sea. *Deep Sea Research Part A. Oceanographic Research Papers*, 38, S875–S882. [https://doi.org/10.1016/S0198-0149\(10\)80014-7](https://doi.org/10.1016/S0198-0149(10)80014-7)
- Luther, G. W., III, Wu, J., & Cullen, J. (1995). Redox chemistry of iodine in seawater: Frontier molecular orbital theory considerations. In C. P. Huang, C. R. O'Melia, & J. J. Morgan (Eds.), *Aquatic chemistry: Interfacial and interspecies processes, Advances in Chemistry Series* (Vol. 244, pp. 135–155). American Chemical Society. <https://doi.org/10.1021/ba-1995-0244.ch006>
- Lyons, T. W., Diamond, C. W., Planavsky, N. J., Reinhard, C. T., & Li, C. (2021). Oxygenation, life, and the planetary system during Earth's middle history: An overview. *Astrobiology*, 21(8), 906–923. <https://doi.org/10.1089/ast.2020.2418>
- Marshall, D., & Anglin, C. D. (2004). CO<sub>2</sub>-clathrate destabilization: A new model of formation for molar tooth structures. *Precambrian Research*, 129(3–4), 325–341. <https://doi.org/10.1016/j.precamres.2003.10.007>
- Mei, M. X. (2005). Preliminary study on sequence-stratigraphic position and origin for molar-tooth structure of the Gaoyuzhuang Formation of Mesoproterozoic at Jixian section in Tianjin. *Journal of Palaeogeography*, 7(4), 437–447. (in Chinese with English abstract).
- Meyer, H. J. (1984). The influence of impurities on the growth rate of calcite. *Journal of Crystal Growth*, 66(3), 639–646. [https://doi.org/10.1016/0022-0248\(84\)90164-7](https://doi.org/10.1016/0022-0248(84)90164-7)
- Milliman, J. D., Freile, D., Steinen, R. P., & Wilber, R. J. (1993). Great Bahama Bank aragonitic muds; mostly inorganically precipitated, mostly exported. *Journal of Sedimentary Research*, 63(4), 589–595. <https://doi.org/10.1306/D4267B81-2B26-11D7-8648000102C1865D>
- Pentecost, A., & Spiro, B. (1990). Stable carbon and oxygen isotope composition of calcites associated with modern freshwater cyanobacteria and algae. *Geomicrobiology Journal*, 8(1), 17–26. <https://doi.org/10.1080/01490459009377875>
- Planavsky, N. J., McGoldrick, P., Scott, C. T., Li, C., Reinhard, C. T., Kelly, A. E., et al. (2011). Widespread iron-rich conditions in the mid-Proterozoic ocean. *Nature*, 477(7365), 448–451. <https://doi.org/10.1038/nature10327>
- Planavsky, N. J., Reinhard, C. T., Wang, X., Thomson, D., McGoldrick, P., Rainbird, R. H., et al. (2014). Low Mid-Proterozoic atmospheric oxygen levels and the delayed rise of animals. *Science*, 346(6209), 635–638. <https://doi.org/10.1126/science.1258410>
- Pollock, M. D., Kah, L. C., & Bartley, J. K. (2006). Morphology of molar-tooth structures in Precambrian carbonates: Influence of substrate rheology and implications for genesis. *Journal of Sedimentary Research*, 76(2), 310–323. <https://doi.org/10.2110/jsr.2006.021>
- Poulton, S. W., & Canfield, D. E. (2011). Ferruginous conditions: A dominant feature of the ocean through Earth's history. *Elements*, 7(2), 107–112. <https://doi.org/10.2113/gselements.7.2.107>
- Pratt, B. R. (1998). Molar-tooth structure in Proterozoic carbonate rocks: Origin from synsedimentary earthquakes, and implications for the nature and evolution of basins and marine sediment. *The Geological Society of America Bulletin*, 110(8), 1028–1045. [https://doi.org/10.1130/0016-7606\(1998\)110<1028:MTSIPC>2.3.CO;2](https://doi.org/10.1130/0016-7606(1998)110<1028:MTSIPC>2.3.CO;2)
- Reinhard, C. T., Planavsky, N. J., Olson, S. L., Lyons, T. W., & Erwin, D. H. (2016). Earth's oxygen cycle and the evolution of animal life. *Proceedings of the National Academy of Sciences*, 113(32), 8933–8938. <https://doi.org/10.1073/pnas.1521544113>
- Riding, R. (2006). Cyanobacterial calcification, carbon dioxide concentrating mechanisms, and Proterozoic–Cambrian changes in atmospheric composition. *Geobiology*, 4(4), 299–316. <https://doi.org/10.1111/j.1472-4669.2006.00087.x>
- Romanek, C. S., Grossman, E. L., & Morse, J. W. (1992). Carbon isotopic fractionation in synthetic aragonite and calcite: Effects of temperature and precipitation rate. *Geochimica et Cosmochimica Acta*, 56(1), 419–430. [https://doi.org/10.1016/0016-7037\(92\)90142-6](https://doi.org/10.1016/0016-7037(92)90142-6)
- Saha, S., Dutt, S., & Barkat, R. (2021). Enigmatic molar-tooth structures (MTS) from Mesoproterozoic Deoban limestone, NW-Lesser Himalaya: Evidence for microbial decay and in-situ precipitation. *Journal of Earth System Science*, 130(2), 1–13. <https://doi.org/10.1007/s12040-021-01606-1>
- Shang, M., Tang, D., Shi, X., Zhou, L., Zhou, X., Song, H., & Jiang, G. (2019). A pulse of oxygen increase in the early Mesoproterozoic ocean at ca. 1.57–1.56 Ga. *Earth and Planetary Science Letters*, 527, 115797. <https://doi.org/10.1016/j.epsl.2019.115797>
- Shen, B., Dong, L., Xiao, S., Lang, X., Huang, K., Peng, Y., et al. (2016). Molar tooth carbonates and benthic methane fluxes in Proterozoic oceans. *Nature Communications*, 7(1), 1–6. <https://doi.org/10.1038/ncomms10317>
- Sherman, A. G., James, N. P., & Narbonne, G. M. (2000). Sedimentology of a late Mesoproterozoic muddy carbonate ramp, northern Baffin Island, Arctic Canada. In J. P. Grotzinger & N. P. James (Eds.), *Precambrian carbonates* (Vol. 65, pp. 275–296). Special Publications of SEPM (Society of Economic Paleontologists and Mineralogists).
- Shields, G. A. (2002). Molar-tooth microspar\*: A chemical explanation for its disappearance 750 Ma. *Terra Nova*, 14(2), 108–113. <https://doi.org/10.1046/j.1365-3121.2002.00396.x>

- Spear, N., Holland, H. D., Garcia-Veigas, J., Lowenstein, T. K., Giegengack, R., & Peters, H. (2014). Analyses of fluid inclusions in Neoproterozoic marine halite provide oldest measurement of seawater chemistry. *Geology*, 42(2), 103–106. <https://doi.org/10.1130/G34913.1>
- Summons, R. E., Franzmann, P. D., & Nichols, P. D. (1998). Carbon isotopic fractionation associated with methylotrophic methanogenesis. *Organic Geochemistry*, 28(7–8), 465–475. [https://doi.org/10.1016/S0146-6380\(98\)00011-4](https://doi.org/10.1016/S0146-6380(98)00011-4)
- Sumner, D. Y., & Grotzinger, J. P. (1996). Were kinetics of Archean calcium carbonate precipitation related to oxygen concentration? *Geology*, 24(2), 119–122. [https://doi.org/10.1130/0091-7613\(1996\)024<0119:WKOACC>2.3.CO;2](https://doi.org/10.1130/0091-7613(1996)024<0119:WKOACC>2.3.CO;2)
- Sumner, D. Y., & Grotzinger, J. P. (2004). Implications for Nearchaean ocean chemistry from primary carbonate mineralogy of the Campbellrand-Malmani Platform, South Africa. *Sedimentology*, 51(6), 1273–1299. <https://doi.org/10.1111/j.1365-3091.2004.00670.x>
- Swart, P. K. (2008). Global synchronous changes in the carbon isotopic composition of carbonate sediments unrelated to changes in the global carbon cycle. *Proceedings of the National Academy of Sciences*, 105(37), 13741–13745. <https://doi.org/10.1073/pnas.0802841105>
- Swett, K., & Knoll, A. H. (1985). Stromatolitic bioherms and microphytolites from the late Proterozoic Draken Conglomerate Formation, Spitsbergen. *Precambrian Research*, 28(3–4), 327–347. [https://doi.org/10.1016/0301-9268\(85\)90037-3](https://doi.org/10.1016/0301-9268(85)90037-3)
- Tang, D., Fu, X., Shi, X., Zhou, L., Zheng, W., Li, C., et al. (2022). Enhanced weathering triggered the transient oxygenation event at ~1.57 Ga. *Geophysical Research Letters*, 49(15), e2022GL099018. <https://doi.org/10.1029/2022GL099018>
- Tang, D., Shi, X., Ma, J., Jiang, G., Zhou, X., & Shi, Q. (2017). Formation of shallow-water glaucony in weakly oxygenated Precambrian ocean: An example from the Mesoproterozoic Tieling Formation in North China. *Precambrian Research*, 294, 214–229. <https://doi.org/10.1016/j.precamres.2017.03.026>
- Tang, D., Shi, X., Wang, X., & Jiang, G. (2016). Extremely low oxygen concentration in mid-Proterozoic shallow seawaters. *Precambrian Research*, 276, 145–157. <https://doi.org/10.1016/j.precamres.2016.02.005>
- Tang, Q., Pang, K., Yuan, X., & Xiao, S. (2020). A one-billion-year-old multicellular chlorophyte. *Nature Ecology & Evolution*, 4(4), 543–549. <https://doi.org/10.1038/s41559-020-1122-9>
- Thompson, J. B., & Ferris, F. G. (1990). Cyanobacterial precipitation of gypsum, calcite, and magnesite from natural alkaline lake water. *Geology*, 18(10), 995–998. [https://doi.org/10.1130/0091-7613\(1990\)018<0995:CPOGCA>2.3.CO;2](https://doi.org/10.1130/0091-7613(1990)018<0995:CPOGCA>2.3.CO;2)
- Thompson, J. B., Schultze-Lam, S., Beveridge, T. J., & Des Marais, D. J. (1997). Whiting events: Biogenic origin due to the photosynthetic activity of cyanobacterial picoplankton. *Limnology & Oceanography*, 42(1), 133–141. <https://doi.org/10.4319/lo.1997.42.1.01033>
- Tian, H., Zhang, J., Li, H., Su, W., Zhou, H., Yang, L., et al. (2015). Zircon LA-MC-ICPMS U-Pb dating of tuff from Mesoproterozoic Gaoyuzhuang Formation in Jixian County of North China and its geological significance. *Acta Geoscientia Sinica*, 36(5), 647–658. (in Chinese with English abstract). <https://doi.org/10.3975/cagsb.2015.05.12>
- Tosti, F., & Riding, R. (2017). Fine-grained agglutinated elongate columnar stromatolites: Tieling Formation, ca 1420 Ma, North China. *Sedimentology*, 64(4), 871–902. <https://doi.org/10.1111/sed.12336>
- Trower, E. J., Lamb, M. P., & Fischer, W. W. (2019). The origin of carbonate mud. *Geophysical Research Letters*, 46(5), 2696–2703. <https://doi.org/10.1029/2018GL081620>
- Wang, C., Lechte, M. A., Reinhard, C. T., Asael, D., Cole, D. B., Halverson, G. P., et al. (2022). Strong evidence for a weakly oxygenated ocean-atmosphere system during the Proterozoic. *Proceedings of the National Academy of Sciences*, 119(6), e2116101119. <https://doi.org/10.1073/pnas.2116101119>
- Wang, H., Chu, X., Liu, B., Hou, H., & Ma, L. (1985). *Atlas of the palaeogeography of China* (p. 143). Cartographic Publishing House. (in Chinese with English abstract).
- Wang, Z., Wang, X., Shi, X., Tang, D., Stüeken, E. E., & Song, H. (2020). Coupled nitrate and phosphate availability facilitated the expansion of eukaryotic life at circa 1.56 Ga. *Journal of Geophysical Research: Biogeosciences*, 125(4), e2019JG005487. <https://doi.org/10.1029/2019JG005487>
- Wei, B., Tang, D., Shi, X., Lechte, M., Zhou, L., Zhou, X., & Song, H. (2021). A pulsed oxygenation in terminal Paleoproterozoic ocean: Evidence from the transition between the Chuanlinggou and Tuanshanzi formations, North China. *Geochemistry, Geophysics, Geosystems*, 22(5), e2020GC009612. <https://doi.org/10.1029/2020GC009612>
- Wille, M., Kramers, J. D., Nägler, T. F., Beukes, N. J., Schröder, S., Meisel, T., et al. (2007). Evidence for a gradual rise of oxygen between 2.6 and 2.5 Ga from Mo isotopes and Re-PGE signatures in shales. *Geochimica et Cosmochimica Acta*, 71(10), 2417–2435. <https://doi.org/10.1016/j.gca.2007.02.019>
- Wörndle, S., Crockford, P. W., Kunzmann, M., Bui, T. H., & Halverson, G. P. (2019). Linking the Bitter Springs carbon isotope anomaly and early Neoproterozoic oxygenation through I/[Ca + Mg] ratios. *Chemical Geology*, 524, 119–135. <https://doi.org/10.1016/j.chemgeo.2019.06.015>
- Wu, M., Fang, H., Sun, L., Shi, X., & Tang, D. (2021). Variations in precipitation pathways of Mesoproterozoic shallow seawater carbonates from North China Platform: Response in seawater redox fluctuations. *Journal of Palaeogeography*, 23(4), 703–722. (in Chinese with English abstract). <https://doi.org/10.7605/gdlxb.2021.04.050>
- Zhang, K., Zhu, X., Wood, R. A., Shi, Y., Gao, Z., & Poulton, S. W. (2018). Oxygenation of the Mesoproterozoic ocean and the evolution of complex eukaryotes. *Nature Geoscience*, 11(5), 345–350. <https://doi.org/10.1038/s41561-018-0111-y>
- Zhang, P., Huang, K. J., Luo, M., Cai, Y., & Bao, Z. (2022). Constraining the terminal Ediacaran seawater chemistry by Mg isotopes in dolostones from the Yangtze Platform, South China. *Precambrian Research*, 377, 106700. <https://doi.org/10.1016/j.precamres.2022.106700>